UBCTP 92-013
Fermilab Library
0 1160 0015990 9

79

UBCTP-92-013

Longitudinal Modes in Quasi-One-Dimensional Antiferromagnets

Ian Affleck[a,b] and Greg F. Wellman[b*]
[a] *Canadian Institute for Advanced Research and* [b] *Physics Department, University of British Columbia, Vancouver, BC, V6T 1Z1, Canada*

FERMILAB
JUN 10 1992
LIBRARY

Neutron-scattering data on $CsNiCl_3$, a quasi-one-dimensional spin-one antiferromagnet, exhibit an anomalous mode. It was later proposed, based on a Landau-Ginsburg model, that this should be viewed as a longitudinal fluctuation of the sub-lattice magnetization. This theory is elaborated in more detail here and compared with experimental data on $CsNiCl_3$ and $RbNiCl_3$. In particular, we give explicitly a renormalization group argument for the existence of such modes in Néel-ordered antiferromagnets which are nearly disordered by quantum fluctuations, due to quasi-one-dimensionality or other effects. We then discuss the non-Néel case of a stacked triangular lattice like $CsNiCl_3$ where longitudinal and transverse modes mix. In this case the quantum disorder transition is driven first order by fluctuations and the longitudinal mode always has a finite width. Effects of a magnetic field on the magnon spectrum are calculated both in conventional spin-wave theory and in the Landau-Ginsburg model and are compared with experimental data on $CsNiCl_3$. This model is compared with an alternative Lagrangian-based one that was proposed recently.

PACS numbers: 75.10.Jm

ROUTE TO
NAME
LOCATION

I. INTRODUCTION

It was first argued by Haldane[1] that one-dimensional integer-spin Heisenberg antiferromagnets have an excitation gap above a singlet groundstate. The first experimental evidence for the Haldane gap was obtained by Buyers et al.[2] in neutron-scattering experiments on $CsNiCl_3$. The spin Hamiltonian for this material is highly isotropic (ie. Heisenberg-like) in spin-space and apparently exhibits a ratio of inter-chain to intra-chain couplings of about 2%. This weak inter-chain coupling produces magnetic order at a temperature of 4.8^0K, about 1/3 of the intra-chain coupling. Because the lattice structure is of stacked triangular type, the ordered state has antiparallel neighboring spins along the chains and neighboring spins at angles of $2\pi/3$ in the planes. (See Figure 1.) Neutron-scattering experiments at temperatures of about 10^0K, above the ordering temperature but still quite small compared to the exchange energy, indicate the existence of a gap in the purely one-dimensional case. Experiments in the ordered phase, below 4.8 ^0K also exhibit anomalous behavior. Apart from the Goldstone modes predicted by spin-wave theory, a portion of another excitation branch with a finite gap is also observed. This was argued[3] to be a longitudinal mode, ie. a longitudinal fluctuation of the sub-lattice magnetization, and a Landau-Ginsburg model was constructed to study the problem. In this model the long-wavelength staggered magnetization field is treated as a three-vector field, $\vec{\phi}$, of arbitrary magnitude and direction in spin-space. In a magnetically ordered state this field has a non-zero groundstate expectation value. In a simple Néel state, as would occur for a bipartite lattice (in which all spins are parallel or anti-parallel) fluctuations in the direction of this field give the usual two Goldstone modes of spin-wave theory. Fluctuations in the magnitude of the field correspond to the longitudinal mode. The neccessity of three modes follows from continuity from the disordered phase where the groundstate expectation value vanishes and

the magnon is a triplet. The stacked triangular lattice is more complicated. Now a transverse fluctuation on one site is not orthogonal to a longitudinal one on a neighboring site in the same plane. Consequently the transverse and longitudinal modes mix in the Landau-Ginsburg model.

The Landau-Ginsburg model predicts that the longitudinal mode has a finite decay rate into a pair of Goldstone modes (even at zero temperature). Consequently it is possible to view the longitudinal mode as a two-magnon resonance, making contact with the traditional Holstein-Primakov approach to spin-wave theory. This decay rate depends on the size of the $|\vec{\phi}|^4$ coupling in the Landau-Ginsburg model. The width to gap ratio vanishes linearly at weak coupling. If this decay rate is too large the longitudinal mode might not be observable. In general the observability of the longitudinal mode is an empirical question, but there is one case where we can predict with confidence that the longitudinal mode is very long-lived. This occurs in the simple Néel case when the system is very close to being disordered by quantum fluctuations. This would correspond to the case where the sub-lattice magnetization is very much reduced compared to its classical value (s) at $T = 0$ due to quantum fluctuation effects. The strength of these fluctuation effects is determined by the spin Hamiltonian. One way of enhancing them is by making the system quasi-one-dimensional. As the ratio of interchain to intrachain couplings is lowered, eventually the order is destroyed, even at $T = 0$. When this ratio is only slightly larger than this critical value the longitudinal mode is very long-lived. This follows from the fact that this second-order, $T = 0$ quantum phase transition is in the four-dimensional universality class and is consequently governed by the weak-coupling Landau-Ginsburg model. [See for example Ma[4].] ie. the model becomes exact, with a very small coupling constant very close to the critical point. Consequently, at the critical point the gap of the longitudinal mode vanishes, as

does the width to gap ratio. Sufficiently close to the critical point, on the ordered side, the longitudinal mode will then be very light and highly stable.

However, the magnetic ordering transition in a stacked triangular antiferromagnet is in a different universality class than the simple Néel case. This can be seen from the fact that a Néel state is invariant under rotations about the unique ordering axis, whereas the triangular state has no such residual $U(1)$ symmetry. A renormalization group analysis in this case indicates that the Gaussian fixed point is unstable.[5] This indicates the occurrance of a fluctuation-induced first-order phase transition. Since the $|\vec{\phi}|^4$ coupling constants do not renormalize to zero in this case, the longitudinal mode does not become perfectly stable.

In general, the question of whether or not the longitudinal mode will be sufficiently narrow to be observed is a heuristic one. It is reasonable to expect it to be more observable for systems which are quite close to the quantum disorder transition.

We emphasize that the renormalization group argument for the stability of the longitudinal mode depends crucially on the fact that the transition is in the four-dimensional universality class, since it occurs at $T = 0$. The finite-temperature transition is, of course, in the three-dimensional universality class and consequently exhibits much less trivial critical behavior. There is no reason to expect a stable longitudinal mode in this case.

The outline of the rest of this paper is as follows. In the next section, we review the Landau-Ginsburg model and the calculation of the dispersion relation for both Néel and triangular cases. We also discuss the extent to which neutron-scattering data on $CsNiCl_3$[2,6] and $RbNiCl_3$[7] agree with this model. While the agreement is not completely satisfactory, we argue that the $CsNiCl_3$ data clearly calls for a non-trivial extension of spin-wave theory. In Section III we give the renormalization group arguments for the stability of the longitudinal mode in the Néel case and

for the first-order nature of the transition in the triangular case. In Section IV we calculate the magnetic field dependence of the magnon dispersion relation, both in ordinary spin-wave theory and in the Landau-Ginsburg model. It is again clear that spin-wave theory fails to capture, even qualitatively, trends in the experimental data.[6] It is unclear how good the agreement with the Landau-Ginsburg model is; a detailed comparison will require the calculation of intensities and lifetimes and more experiments. The final section summarizes the agreement between experiment and theory. The appendix compares the Landau-Ginsburg model to another one which was recently proposed.[8]

II. LANDAU-GINSBURG MODEL

We begin by discussing a single chain, Heisenberg antiferromagnet:

$$H_1 = 2J \sum_i \vec{S}_i \cdot \vec{S}_{i+1} \tag{2.1}$$

The continuum limit is defined by introducing[1] the pair of non-commuting vector fields, $\vec{\phi}(z)$ and $\vec{l}(z)$ representing the long-wavelength staggered and uniform magnetization, respectively. (z measures distance along the chain. We set the lattice spacing equal to one for the time being.) Because the integral of $\vec{l}$ over the entire chain gives the conserved total magnetization, its commutation relations are fixed to be:

$$\begin{aligned} [l^i(z), l^j(z')] &= i\epsilon^{ijk} l^k(z)\delta(z-z') \\ [l^i(z), \phi^j(z')] &= i\epsilon^{ijk} \phi^k(z)\delta(z-z') \end{aligned} \tag{2.2}$$

(We set $\hbar = 1$.) The commutation relations of the components of $\vec{\phi}$ with themselves are not fixed by any symmetry requirement and depend on the spin-magnitude,

s. We make the large-s semi-classical approximation that they commute. A correct treatment of the large-s limit also requires that we impose the constraints, $|\vec{\phi}|^2 - (\vec{l})^2/s^2 \approx (\vec{\phi})^2 = 1$, $\vec{\phi} \cdot \vec{l} = 0$. This defines the non-linear sigma-model, upon expanding the hamiltonian to second order in $\vec{l}$ and $d\vec{\phi}/dz$. A perturbative treatment of the σ-model involves expanding $\vec{\phi}$ about its groundstate expectation value. This gives two Goldstone modes, the same spectrum as obtained from spin-wave theory (at long wavelengths). However, this is known to be completely the wrong picture in one dimension. Quantum fluctuations disorder the groundstate. Roughly speaking, $\vec{\phi}$ fluctuates around the unit sphere so that $< 0|\vec{\phi}|0 >= 0$. The spectrum consists of a triplet of massive magnons which correspond to the three components of $\vec{\phi}$. [Since the field theory is Lorentz-invariant, the magnon dispersion has the relativistic form $E(Q - \pi) = \sqrt{(vQ)^2 + \Delta^2}$, where Q is the momentum, Δ the gap and $v \approx 4Js$ the spin-wave velocity. Thus we may regard Δ/v^2 as the rest-mass.] The Landau-Ginsburg model is designed to give the correct behavior at a mean-field level.[3] We simply relax the constraint on $\vec{\phi}$ and replace it by a quadratic plus quartic potential. The full Lagrangian density is given by:

$$\mathcal{L}_1 = \frac{1}{2v}\left(\frac{\partial\vec{\phi}}{\partial t}\right)^2 - \frac{v}{2}\left(\frac{\partial\vec{\phi}}{\partial z}\right)^2 - \frac{\Delta^2}{2v}|\vec{\phi}|^2 - \frac{\lambda}{4}|\vec{\phi}|^4 \tag{2.3}$$

The quartic term is, in general, neccessary for stability. The uniform magnetization density is then determined from the commutation relations to be:

$$\vec{l} = (1/v)\vec{\phi} \times \partial\vec{\phi}/\partial t \tag{2.4}$$

This model becomes essentially exact in the large-n limit of the $O(n)$ σ-model. We may estimate the normalization factor for the staggered magnetization as: $\vec{S}_i \approx (-1)^i s\sqrt{g}\vec{\phi}$ where $g \approx \sqrt{2/s}$, based on the large-n and large-s limits.

We now consider a quasi-one-dimensional system:

$$H_3 = J \sum_{<i,j>}^{chains} \vec{S}_i \cdot \vec{S}_j + J' \sum_{<i,j>}^{planes} \vec{S}_i \cdot \vec{S}_j \tag{2.5}$$

Here the first term is over all nearest neighbor pairs on the same chain and the second is over all nearest neighbor pairs in the same plane, with $J' << J$. (Each nearest neighbor pair occurs *twice* in the above sums.) The Landau-Ginsburg Lagrangian is obtained by introducing a separate field $\vec{\phi}_i(z)$ for each chain, i and then coupling the staggered magnetization vectors at adjacent points on neighboring chains. (A coupling of uniform magnetizations could also be included but this leads to corrections of higher order in J'/J and, in any event, does not qualitatively alter our conclusions.) Thus the three-dimensional Lagrangian is given by:

$$L_3 = \int dz \Big\{ \sum_i \mathcal{L}_1[\vec{\phi}_i(z)] - 2J's \sum_{<i,j>} \vec{\phi}_i(z) \cdot \vec{\phi}_j(z) \Big\} \tag{2.6}$$

Here the second sum is over nearest neighbor chains. In the ordered state $< \vec{\phi}_i(z) >$ will be constant along each chain. Dropping the t and z derivitive terms the Lagrangian becomes minus the potential energy. We see that whether or not order occurs is determined by a competition between the Haldane gap, Δ and the interchain coupling J'. The critical value of J' is $O(\Delta^2/vs)$. In the disordered phase, at small J' where $< 0|\vec{\phi}|0 >= 0$, we calculate the magnon dispersion relation by simply ignoring the quartic term. We see that there is a triplet of massive magnons with a dispersion relation:

$$E_{triplet}(Q_z - \pi, \vec{Q}_\perp) = \sqrt{v^2 Q_z^2 + \Delta^2 + 8J'vsf(\vec{Q}_\perp)} \tag{2.7}$$

where

$$f\vec{Q}_\perp) = (1/2)\sum_i e^{i\vec{Q}_\perp\cdot\vec{\delta}_i} \tag{2.8}$$

and the sum runs over the vectors, $\vec{\delta}_i$ to nearest neighbor sites in the planar lattice (assumed to be Bravais). This formula is valid for $Q_z \approx \pi$. The shift of Q_z by π is due to the fact that $\vec{\phi}$ is the *staggered* magnetization.

Let us now consider the ordered phase, which occurs for sufficiently large J'. We now must distinguish between different lattice types. We first consider the case of a tetragonal lattice; ie. a square lattice of chains. (The following discussion could be trivially generalized to the case where the transverse lattice is rectangular rather than square.) The ordered groundstate is the simple Néel state with all nearest neighbor spins anti-parallel. Writing,

$$< \phi_i >= \pm\phi_0\hat{z} \tag{2.9}$$

on the two sub-lattices, the potential energy per spin becomes:

$$V(\phi_0) = (\Delta^2/2v - 8J's)\phi_0^2 + (\lambda/4)\phi_0^4 \tag{2.10}$$

We see that the critical value of J' is

$$J'_c = \Delta^2/16vs \tag{2.11}$$

For larger J' the size of the sub-lattice magnetization is given by:

$$\phi_0^2 = (16J's - \Delta^2/v)/\lambda \tag{2.12}$$

We expand L to second order in small fluctuations:

$$\vec{\phi} = (\phi_x, \phi_y, \phi_0 + \phi_z) \tag{2.13}$$

x and y fluctuations are transverse and z-fluctuations are longitudinal. These do not mix to quadratic order. We may then read off the dispersion relations:

$$E_t(Q_z - \pi, \vec{Q}_\perp) = \sqrt{v^2 Q_z^2 + 8J'vs[2 + f(\vec{Q}_\perp)]} \tag{2.14}$$

$$E_L(Q_z - \pi, \vec{Q}_\perp) = \sqrt{v^2 Q_z^2 + 8J'vs[2 + f(\vec{Q}_\perp)] + \Delta_L^2} \tag{2.15}$$

where:

$$\Delta_L \equiv \sqrt{2v\lambda\phi_0^2} = \sqrt{2(16J'vs - \Delta^2)} = \sqrt{32vs(J' - J'_c)} \tag{2.16}$$

For the square lattice of chains, of spacing a,

$$f(\vec{Q}_\perp) \equiv cos(aQ_x) + cos(aQ_y) \geq -2 \tag{2.17}$$

Note that E_t vanishes at the antiferromagnetic wave-vector $(\pi/a, \pi/a, \pi)$. E_L, on the other hand, has a gap, Δ_L at this wave-vector. Note that all three dispersion relations, that of the triplet in the disordered phase, Eq.(2.7), and those of the longitudinal mode and transverse modes in the ordered phase, Eq. (2.15) becomes identical at $J' = J'_c$. ie. as we vary J', the spectrum varies continuously, the triplet of the disordered phase splitting up into the two transverse modes and one longitudinal mode of the ordered phase.

The intensities of these modes take a very simple form. The canonical commutation relations, $[\phi(x,t), \dot{\phi}(x',t)] = iv\delta(x - x')$, implies that the spin correlation function is

$$S^{aa}(Q_z-\pi,\vec{Q}_\perp,E) \equiv < S^a S^a > (Q_z-\pi,\vec{Q}_\perp,E) \propto < \phi^a \phi^a > (\vec{Q},E) \propto \delta[E-E_a(\vec{Q})]/E^a(\vec{Q}) \tag{2.18}$$

{To obtain the neutron-scattering cross-section S^{aa} must be multiplied by the Lorentz factor $(1-\hat{Q}_a^2)$, and a sum over a must be performed, depending on polarization.} Thus, in particular, the intensity of the transverse modes ($a = 1,2$) blows up at the ordering wave-vector, whereas the intensity of the longitudinal mode remains finite. The transverse modes would appear in xy-polarized experiments and the longitudinal mode in z polarized experiments. As we shall see, things are considerably more complicated in the case of a stacked-triangular lattice.

The transverse modes are simply the standard result of linear spin-wave theory[9], for $Q \approx \pi$ and $J' << J$. To see this note that the standard spin-wave theory spectrum is:

$$E_{SWT}(\vec{Q}) = \sqrt{(4Js+8J's)^2 - [4Js\ cosQ_z + 4J's f(\vec{Q}_\perp)]^2} \tag{2.19}$$

Expanding to first order in J'/J and Q_z^2 inside the square root, and using $v = 4Js$, we obtain precisely the first of Eqs. (2.15). The longitudinal mode, on the other hand, is not a standard spin-wave theory result. The reason is that in spin-wave theory the spins are considered to be of fixed length, as in the non-linear σ-model. The longitudinal mode occurs in the above treatment simply because we have relaxed the constraint on the magnitude of the field $\vec{\phi}$ in passing to the Landau-Ginsburg model. Actually, the two theories are not quite as different as they at first appear. To see this note that the longitudinal mode is unstable, even at zero temperature. It can always decay into a pair of transverse modes (ie. Goldstone bosons). This is

kinematically allowed since the Goldstone modes are gapless whereas the longitudinal mode has a gap. It is allowed by conservation of the z-component of total spin, since the longitudinal mode has $\mathcal{S}^z = 0$ whereas the two species of transverse modes have $\mathcal{S}^z = \pm 1$. Decay into a pair of Goldstone modes of opposite spin conserves spin. Such a decay vertex occurs in the theory due to the $(\lambda/4)|\vec{\phi}|^4$ term in the Lagrangian. Expanding $\vec{\phi}$ as in Eq. (2.13) we obtain a cubic term:

$$\mathcal{L}_{cubic} = -\lambda\phi_0\phi_z(\phi_x^2 + \phi_y^2) \tag{2.20}$$

We see that the decay rate, which goes like the square of this coupling constant, is of $O(\lambda)$. The Landau-Ginsburg model actually reduces to the non-linear σ-model in the limit where $\lambda \to \infty$ and $\Delta^2 \to -\infty$ with $-\Delta^2/\lambda = 1$, since then the magnitude of $\vec{\phi}$ is forced to be exactly one. In this limit the mass of the longitudinal mode goes to infinity, as does its decay rate. How light and narrow the longitudinal mode is depends on the parameters in the model. In particular, its mass is controlled by $J' - J'_c$ and its width by λ. We expect that spin-wave theory will exhibit a two-magnon resonance with a finite energy gap. This resonance may then be identified with the longitudinal mode. Whether or not the longitudinal mode is stable enough to observe depends on the parameter λ in the Landau-Ginsburg model. We will argue, using the renormalization group, in the next section, that the width to gap ratio of the longitudinal mode vanishes in the limit $J' \to J'_c$. This corresponds to the fact that the renormalized coupling constant λ vanishes at the critical point.

We now consider the effects of anisotropy. If we consider axial anisotropy which breaks the $SU(2)$ symmetry down to a $U(1)$ subgroup, rotation about the z-axis, then we must distinguish the easy-plane and easy-axis case. In the first case, the $U(1)$ symmetry is spontaneously broken so there is a single Goldstone mode. Again

the longitudinal mode is unstable against decaying into the Goldstone mode. In the second, easy-axis case, the $U(1)$ symmetry is *not* spontaneously broken in the ordered phase, only the Z_2 symmetry $S^z \to -S^z$ is broken. Consequently there are no gapless Goldston modes. Spin-wave theory and the Landau-Ginsburg model predict that the two branches of would-be Goldstone modes have equal gaps. However, according to the Landau-Ginsburg model, the longitudinal mode still has vanishing gap at the critical value of J', and thus becomes lighter than the would-be Goldstone modes sufficiently close to the critical point (on the ordered side). Therefore it becomes kinematically unable to decay in this region and should exist as an infinitely stable excitation.

We now turn to the case of a triangular lattice of chains. We choose the triangular lattice to lie in the xy-plane with links parallel to the x-axis, as shown in Figure 2. The lattice spacing is a. The spacing between spins along the chains we take to be $c/2$, in order to agree with standard conventions for $CsNiCl_3$ which has two formula units per unit cell. We choose a basis of primitive lattice vectors:

$$\begin{aligned}
\vec{a}_1 &\equiv (a/2, -\sqrt{3}a/2, 0) \\
\vec{a}_2 &\equiv (a/2, \sqrt{3}a/2, 0) \\
\vec{a}_3 &\equiv (0, 0, c)
\end{aligned} \tag{2.21}$$

It is also convenient to define a set of three linearly dependent in-plane lattice vectors, $\vec{\delta}_i$, with $i = 1, 2, 3$:

$$\begin{aligned}
\vec{\delta}_1 &\equiv \vec{a}_1 \\
\vec{\delta}_2 &\equiv \vec{a}_2
\end{aligned}$$

$$\vec{\delta}_3 \equiv -\vec{a}_1 - \vec{a}_2 = (-a, 0, 0) \tag{2.22}$$

(See Figure 2.) The reciprocal lattice is also triangular. The primitive vectors, $\vec{b}_i$, $i = 1, 2, 3$, defined by the conditions:

$$\vec{b}_i \cdot \vec{a}_j = 2\pi\delta_{ij} \tag{2.23}$$

are given by:

$$\begin{aligned}
\vec{b}_1 &\equiv \frac{4\pi}{\sqrt{3}a}\left(\frac{\sqrt{3}}{2}, \frac{-1}{2}, 0\right) \\
\vec{b}_2 &\equiv \frac{4\pi}{\sqrt{3}a}\left(\frac{\sqrt{3}}{2}, \frac{1}{2}, 0\right) \\
\vec{b}_3 &\equiv \frac{2\pi}{c}\left(0, 0, 1\right)
\end{aligned} \tag{2.24}$$

(See Figure 3.) Wave-vectors are expanded in reciprocal lattice vectors:

$$\vec{Q} = (Q_1, Q_2, Q_3) \equiv \sum_{i=1}^{3} Q_i \vec{b}_i \tag{2.25}$$

We also sometimes refer to wave-vectors by x, y and z-components, and use $\vec{Q}_\perp$ to label the projection of the wave-vector onto the basal plane. The classical ordered state now involves three different directions, making angles of $2\pi/3$ with each other. We choose these to lie in the xz-plane, with one of them lying along the z-axis, in agreement with the conventions of previous work. See Figure 1. Hence the classical state at lattice point $\vec{x}_i$ is given by:

$$\vec{S}_i = s(sin\vec{Q}_0 \cdot \vec{x}_i, 0, cos\vec{Q}_0 \cdot \vec{x}_i) \tag{2.26}$$

where the ordering wave-vector, $\vec{Q}_0$, is given by:

$$\vec{Q}_0 \equiv (1/3, 1/3, 1) \tag{2.27}$$

in the notation of Equation (2.25). It is also convenient to define the projection of the ordering wave-vector onto the basal (xz) plane, $\vec{Q}_2$:

$$\vec{Q}_2 \equiv (1/3, 1/3, 0) \tag{2.28}$$

Note that $\vec{Q}_2$ lies on the x-axis, at a corner of the paramagnetic Brillouin zone, which is a hexagon, as shown in Figure 3.

The inter-chain coupling term in the Lagrangian is now of the form:

$$L_{ic} = -(4J'/c) \sum_{<i,j>} \int dz \vec{\phi}_i(z) \cdot \vec{\phi}_j(z) \tag{2.29}$$

Noting that for two neighboring chains, $\vec{\phi}_i \cdot \vec{\phi}_j = -(1/2)\phi_0^2$ and that each chain has six nearest neighbor chains, we find the potential energy per chain, per unit length, in the ordered state:

$$V(\phi_0) = (\Delta^2/2v - 12J's/c)\phi_0^2 + (\lambda/4)\phi_0^4 \tag{2.30}$$

Now the critical value of J' is:

$$J'_c = \Delta^2 c/24vs \tag{2.31}$$

and the sub-lattice magnetization in the ordered state, for $J' > J'_c$ is:

$$\phi_0^2 = (24J's/c - \Delta^2/v)/\lambda \tag{2.32}$$

To obtain the excitation spectrum we expand the Lagrangian density to quadratic order in small fluctuations around the ordered state. For this purpose, it is convenient to introduce two orthogonal unit vectors, both lying in the zx-plane in spin-space, at each lattice site, i, $\hat{e}_{Li}$ and $\hat{e}_{1i}$. $\hat{e}_{Li}$ is parallel to $< \vec{\phi}_i >$ and $\hat{e}_{1i}$ is perpendicular to it. [See Figure 4.] In terms of the projection of the ordering wave-vector onto the basal plane, $\vec{Q}_2$, we may write:

$$\begin{aligned} \hat{e}_{Li} &\equiv (sin\vec{Q}_2 \cdot \vec{x}_i, 0, cos\vec{Q}_2 \cdot \vec{x}_i) \\ \hat{e}_{1i} &\equiv (cos\vec{Q}_2 \cdot \vec{x}_i, 0, -sin\vec{Q}_2 \cdot \vec{x}_i) \end{aligned} \tag{2.33}$$

Introducing the transverse xz-fluctuation, ϕ_{1i}, the transverse y-fluctuation, ϕ_{2i} and the longitudinal (xz) fluctuation ϕ_{Li}, as well as the unit vector parallel to the y-axis, $\hat{e}_2$, we decompose the field at each site as:

$$\vec{\phi}_i = \hat{e}_{Li}(\phi_0 + \phi_{Li}) + \hat{e}_{1i}\phi_{1i} + \hat{e}_2\phi_{2i} \tag{2.34}$$

We now substitute this decomposition into the Lagrangian, Eq. (2.6) and expand to quadratic order in ϕ_1, ϕ_2 and ϕ_L. It is important to note that we obtain cross-terms between the transverse xz-mode, ϕ_1 and the longitudinal mode ϕ_L. This does not occur in the case of a bipartite lattice. It occurs here because longitudinal and transverse fluctuations on neighboring sites are not orthogonal to each other as illustrated in Figure 5. On the other hand the transverse y-mode, ϕ_2, is unmixed (to quadratic order). The terms quadratic in the y-mode are:

$$\mathcal{L}_y = \sum_i [\frac{1}{2v}\left(\frac{\partial\phi_{2i}}{\partial t}\right)^2 - \frac{v}{2}\left(\frac{\partial\phi_{2i}}{\partial z}\right)^2 - \frac{\Delta^2}{2v}\phi_{2i}^2 - \frac{\lambda}{2}\phi_0^2\phi_{2i}^2] + \frac{4J's}{c}\sum_{<i,j>}\phi_{2i}\phi_{2j} \tag{2.35}$$

The terms quadratic in the transverse and longitudinal xz-modes are:

$$\mathcal{L}_{xz} = \sum_i [\frac{1}{2v}\left(\frac{\partial \phi_{1i}}{\partial t}\right)^2 - \frac{v}{2}\left(\frac{\partial \phi_{1i}}{\partial z}\right)^2 - \frac{\Delta^2}{2v}\phi_{1i}^2 + \frac{1}{2v}\left(\frac{\partial \phi_{Li}}{\partial t}\right)^2 - \frac{v}{2}\left(\frac{\partial \phi_{Li}}{\partial z}\right)^2 - \frac{\Delta^2}{2v}\phi_{Li}^2$$
$$-\frac{\lambda}{2}\phi_0^2(\phi_{1i}^2 + 3\phi_{Li}^2)] - (4J's/c)\sum_{<i,j>}[(-1/2)\phi_{1i}\phi_{1j} + (-1/2)\phi_{Li}\phi_{Lj}$$
$$+(\hat{e}_{Li}\cdot\hat{e}_{1j})\phi_{Li}\phi_{1j} + (\hat{e}_{1i}\cdot\hat{e}_{Lj})\phi_{1i}\phi_{Lj}] \tag{2.36}$$

Here we have used the fact that $\hat{e}_{Li}\cdot\hat{e}_{Lj} = \hat{e}_{1i}\cdot\hat{e}_{1j} = -1/2$ for nearest neighbor sites. The other dot products, $\hat{e}_{1i}\cdot\hat{e}_{Lj}$, take on the values $\pm\sqrt{3}/2$. In terms of the lattice vectors, $\vec{\delta}_i$, [see Equation (2.22)] the inter-chain term in $\mathcal{L}_{xz}$ can be written:

$$\mathcal{L}_{xz,ic} = -(4J's/c)\sum_i\sum_{b=1}^{3}\sum_{\pm}\{(-1/2)[\phi_1(\vec{x}_i)\phi_1(\vec{x}_i \pm \vec{\delta}_b) + \phi_L(\vec{x}_i)\phi_L(\vec{x}_i \pm \vec{\delta}_b)]$$
$$\mp(\sqrt{3}/2)[\phi_1(\vec{x}_i)\phi_L(\vec{x}_i \pm \vec{\delta}_b) - \phi_L(\vec{x}_i)\phi_1(\vec{x}_i \pm \vec{\delta}_b)]\} \tag{2.37}$$

At this point we Fourier transform. It is convenient to define Fourier modes, $\vec{\phi}(\vec{Q})$, over the entire paramagnetic Brillouin zone in the basal plane, shown in Figure 3. In this way, we only obtain three branches of excitations, corresponding to ϕ_2 and two linear combinations of ϕ_1 and ϕ_L. Of course the basal plane antiferromagnetic Brillouin zone has only 1/3 the area so there should be 3 times as many excitation branches. This simplifying step is possible because of the symmetry of the antiferromagnetic groundstate under simultaneous translation by one lattice spacing and rotation of the spins by $2\pi/3$ about the y-axis. This symmetry is incorporated into the definition of the components ϕ_1 and ϕ_L via the rotating co-ordinate system, $\hat{e}_1$ and $\hat{e}_L$. To obtain the experimentally observable neutron-scattering cross-section,

we must translate the xz branches into the antiferromagnetic zone, giving a total of 5 branches. Explicitly, we see from Eq. (2.33) that:

$$\vec{\phi}(\vec{Q}) \approx \{ \sum_{n=-1}^{1} [-ni\phi_L(\vec{Q}+n\vec{Q}_2)+\phi_1(\vec{Q}+n\vec{Q}_2)]/2, \phi_2(\vec{Q}), \sum_{n=-1}^{1} [\phi_L(\vec{Q}+n\vec{Q}_2)+ni\phi_1(\vec{Q}+n\vec{Q}_2)]/2\} \tag{2.38}$$

We find that the dispersion relation for the y-mode is given by:

$$E_2(Q_z - 2\pi/c, \vec{Q}_\perp) = \sqrt{(vQ_z)^2 + (8vJ's/c)[3 + 2f(\vec{Q}_\perp)]} \tag{2.39}$$

where now:

$$f(\vec{Q}_\perp) \equiv cos(2\pi Q_1) + cos(2\pi Q_2) + cos[2\pi(Q_1 + Q_2)] \tag{2.40}$$

The two xz modes are given by the solution of the eigenvalue equation:

$$\begin{pmatrix} (vQ_z)^2 + (8J'sv/c)(3-f) & i8\sqrt{3}J'sv\tilde{f}/c \\ -i8\sqrt{3}J'sv\tilde{f}/c & (vQ_z)^2 + (8J'sv/c)(3-f) + \Delta_L^2 \end{pmatrix} \begin{pmatrix} \tilde{\phi}_1 \\ \tilde{\phi}_L \end{pmatrix} = E^2 \begin{pmatrix} \tilde{\phi}_1 \\ \tilde{\phi}_L \end{pmatrix} \tag{2.41}$$

where

$$\tilde{f}(\vec{Q}_\perp) \equiv sin(2\pi Q_1) + sin(2\pi Q_2) + sin[2\pi(Q_1 + Q_2)] \tag{2.42}$$

Note that this is a slightly different notation than in Ref. (3).

$$\Delta_L^2 \equiv 48J'vs/c - 2\Delta^2 \tag{2.43}$$

The two frequencies are:

$$E_{\pm}^2(Q_z-2\pi/c,\vec{Q}_\perp) = (vQ_z)^2+(8J'vs/c)(3-f(\vec{Q}_\perp)+\Delta_L^2/2\pm\sqrt{(\Delta_L^2/2)^2+3[8J'sv\tilde{f}(\vec{Q}_\perp)/c]^2} \tag{2.44}$$

The intensities of the modes, can be calculated from the eignenvectors obtained from Eq. (2.41). Normalizing the eigenvectors to one: $|\tilde{\phi}_1|^2 + |\tilde{\phi}_L|^2 = 1$, we may write:

$$\begin{aligned}
\mathcal{S}^{yy}(Q_z - 2\pi/c, \vec{Q}_\perp, E) &\propto \frac{1}{E_2(\vec{Q})}\delta[E - E_2(\vec{Q})] \\
\mathcal{S}^{xx}(Q_z - 2\pi/c, \vec{Q}_\perp, E) &= \mathcal{S}^{zz}(Q_z - 2\pi/c, \vec{Q}_\perp, E) \\
&\propto \frac{1}{4}\sum_{\pm}\sum_{n=-1}^{1}\frac{|\tilde{\phi}_{1\pm} - ni\tilde{\phi}_{L\pm}|^2}{E_\pm}(\vec{Q}+n\vec{Q}_2)\delta[E - E_\pm(\vec{Q}+n\vec{Q}_2)]
\end{aligned} \tag{2.45}$$

The shift of $\vec{Q}$ by $n\vec{Q}_2$ ($n = \pm 1$) results from the rotating coordinate system implicit in the definition of ϕ_1 and ϕ_L, see Eq. (2.38). The constants of proportionality are the same in both of the above equations. Finally, solving the eigenvalue equation, Equation (2.41), we obtain

$$|\tilde{\phi}_{1\pm} - ni\tilde{\phi}_{L\pm}|^2 = \frac{\left[8\sqrt{3}J'sv\tilde{f}/c - n\left(\Delta_L^2/2 \mp \sqrt{(\Delta_L^2/2)^2+3[8J'sv\tilde{f}/c]^2}\right)\right]^2}{(8\sqrt{3}J'sv/c\tilde{f})^2 + \left(\Delta_L^2/2 \mp \sqrt{(\Delta_L^2/2)^2+3[8J'sv\tilde{f}/c]^2}\right)^2} \tag{2.46}$$

We see from its definition, Eq. (2.43) that $\Delta_L^2 < 48J'vs/c$ provided that $\Delta^2 > 0$. However, Δ^2 must be regarded as a renormalized parameter and, for sufficiently large J'/J it may become negative. Therefore, it is interesting to consider the qualitative behavior of this spectrum as a function of the parameter Δ_L^2 for $0 <$

$\Delta_L^2 < \infty$, with J' held fixed. Let us first consider the limit, $\Delta_L^2 \to \infty$. In this limit, $E_+ \to \infty$ and $E_-^2 \to (vQ_z)^2 + (8J'vs/c)(3 - f(\vec{Q}_\perp))$. In this limit, E_- becomes purely transverse and E_+ purely longitudinal. This limiting formula for E_- can be seen to be the same as that of conventional spin-wave theory in the limit of small $Q_z - 2\pi/c$ and small J'/J. Likewise, the y-mode, which is unaffected by Δ_L^2, has the same dispersion relation as the corresponding mode in conventional spin-wave theory in this limit. However, as we reduce Δ_L^2, the transverse xz fluctuations mix increasingly with longitudinal fluctations so that E_- deviates from the spin-wave theory result. Likewise the other branch, of energy E_+ moves down in energy. Finally, at $J' = J'_c$, $\Delta_L^2 = 0$ and the xz-energies become:

$$E_\pm^2(Q_z - 2\pi/c, \vec{Q}_\perp) \to (vQ_z)^2 + (8J'sv/c)[3 - f(\vec{Q}_\perp) \pm \sqrt{3}|\tilde{f}(\vec{Q}_\perp)|] \tag{2.47}$$

Using the identity:

$$f(\vec{Q}_\perp) \pm \sqrt{3}\tilde{f}(\vec{Q}_\perp) = -2f(\vec{Q}_\perp \pm \vec{Q}_2) \tag{2.48}$$

we see that:

$$E_\pm^2(Q_z - 2\pi/c, \vec{Q}_\perp) \to (vQ_z)^2 + (8J'sv/c)[3 + 2f(\vec{Q}_\perp \mp \epsilon\vec{Q}_2)] \tag{2.49}$$

where $\epsilon \equiv sn[\tilde{f}(\vec{Q}_\perp)]$. Comparing with Eq. (2.39) and Eq. (2.7), we see that $E_{triplet}(\vec{Q})$, $E_2(\vec{Q})$ and $E_\pm(\vec{Q} \pm \epsilon\vec{Q}_2)$ all become identical at $J' = J'_c$. Furthermore, in this limit the eigenfunctions take on the simple form $\phi_{L\pm} = \mp\epsilon i\phi_{1\pm} = 1/\sqrt{2}$. Thus, in the formula for the neutron-scattering intensity, Eq. (2.45), two of the terms vanish and the other two become identical, giving: $\mathcal{S}^{xx}(\vec{Q}, E) = \mathcal{S}^{zz}(\vec{Q}, E) = \mathcal{S}^{yy}(\vec{Q}, E)$ at $\Delta_L^2 = 0$. The neutron-scattering cross-section in the ordered phase

goes over continuously to that of the disordered phase. Note that the way this occurs is that the intensity of two of the five branches goes to zero and the other three become degenerate, with zero gap in the limit $\Delta_L^2 \to 0$. For a relatively small value of Δ_L we should expect two of the five branches to be very weak and the other three to lie quite close to each other.

The theoretical spectrum is compared with the experimental results[2,6] on $CsNiCl_3$ in Figure 6. The theory contains three parameters, v, J' and Δ_L. These can be used to fit the slope, $\partial E/\partial Q_z(\vec{Q}_0)$, the bandwidth of the basal plane dispersion at $Q_z = 2\pi/c$ and the gap of the stronger mode of non-zero energy at the ordering wave-vector (ie. $E_-(\vec{b}_3 + 2\vec{Q}_2)$. This procedure gives: $2v/h_P c \approx 1.38THz.$, $J'/h_P = .0052THz$ and $\Delta_L/h_P = .28THz$. (h_P is Planck's constant; we attach the subscript P, to distinguish it from the magnetic field. We follow the standard convention in the neutron-scattering literature of quoting frequencies, rather than angular frequencies; hence they must be multiplied by h_P, not $\hbar$ to obtain the corresponding energies.) Given the weak intensity of two of the branches, as shown in Figure 7, the agreement between theory and experiment is fairly satisfactory. The main discrepancy is that the second xz branch, $E_+(\vec{Q}+\vec{Q}_2) \equiv E_2$ [See Figure 6b] is only resolved for small $\vec{Q}_\perp$ where its energy is about 10% lower than the theoretical prediction. It is important to realize that various effects (such as perturbative corrections from the $\lambda\vec{\phi}^4$-term in the Lagrangian) will renormalize the dispersion relation. It may well be that these effects reduce the energy, E_2 sufficiently that it can only be resolved from E_3 at small $Q_\perp$. The prediction of normal spin-wave theory is compared with experiment in Figure 8. Here we use $J/h_P = (1/4)(2v/c) = .345THz$ and the same value of J' as above. Both theories fit the y-mode quite well; indeed they make essentially identical predictions. However, conventional spin-wave theory disagrees badly with the observed xz-dispersion. Of course, there are also renormalizations of spin-wave

theory, which can be calculated in a $1/s$ expansion using the Holstein-Primakov or Dyson-Maleev formalism. Is it possible that these might eventually lead to good agreement between theory and experiment?

In fact there is a qualitative feature of the data which conventional spin-wave theory will not be able to capture including arbitrary higher-order corrections. This is the striking fact that the energy of the xz-polarized mode observed at $\vec{Q}_\perp = 0$ is at about $2\frac{1}{2}$ times higher energy than that of the upper mode at the ordering wave-vector. Spin-wave theory predicts that these two frequencies should be equal. Furthermore, this is actually a consequence of a symmetry and thus should survive all higher-order corrections. The symmetry argument is most easily understood by plotting the xz-mode in the entire paramagnetic Brillouin zone. The observed neutron-scattering intensity is then obtained by translating this branch into the reduced zone, $\vec{Q} \to \vec{Q} \pm \vec{Q}_2$. The paramagnetic reciprocal lattice is shown in Figure 3. The experimental results shown in Figure 6 correspond to moving along the x-axis, $Q_x = 4\pi\eta/a$, shown in Figure 3. Note that a link of the reciprocal lattice is a perpindicular bisector of this line, cutting it at $\eta = 1/2$. This implies that the dispersion relation is symmetric about $\eta \to 1 - \eta$. The fact that the excitations can be defined over the entire paramagnetic Brillouin zone is a consequence of the symmetry of the antiferromagnetic groundstate under combined translation by one site and rotation by $2\pi/3$. The symmetry $\eta \to 1-\eta$ is a consequence of a symmetry of the paramagnetic Brillouin zone. Thus we expect this symmetry to survive all higher order corrections. Upon translating the spectrum into the antiferromagnetic zone, this symmetry implies that the upper xz branch is symmetric about $\eta = 1/6$ and, in particular, implies the equality of the energies of the upper xz-mode at (1/3,1/3,1) and the xz-mode at (0,0,1). Any model which predicts a single xz branch in the paramagnetic zone, will predict that these energies are equal. [This

includes the alternative model[8] discussed in the appendix.] Thus the observed marked difference in these energies indicates that there are two different xz branches in the paramagnetic zone, as predicted by the Landau-Ginsburg model. Note that this model also obeys the same symmetry. Both xz-branches have the feature that the upper energy (upon translating into the antiferromagnetic zone) at (1/3,1/3,1) is degenerate with the energy at (0,0,1).

$RbNiCl_3$ is another $s = 1$ quasi-one-dimensional Heisenberg antiferromagnet with properties very similar to those of $CsNiCl_3$. The only importance difference appears to be that the ratio of interchain to intrachain couplings is about 80% higher in $RbNiCl_3$. So far, only unpolarized neutron scattering experiments have been reported on this compound.[7] They exhibit a dispersion relation very similar to that of $CsNiCl_3$. Again only a single spin-wave energy is observed near $(0, 0, 1)$. Again this energy is considerably higher than that of the upper mode at $(1/3, 1/3, 1)$. However, in this case it is higher by a factor of approximately 2 rather than $2\frac{1}{2}$. A fit can be obtained to the Landau-Ginsburg model, this time with $2v/h_P c = 1.94 THz$, $J'/h_P = .0143\ THz$ and $\Delta_L/h_P = .9\ THz$, corresponding to a negative value of Δ^2, perhaps indicative of large renormalization effects due to the interchain coupling. The agreement between theory and experiment seems to suffer from the same defect as in $CsNiCl_3$. See Figure 9 and 10. Branch number 2 of Figure 9 is again not observed near $(1/3, 1/3, 1)$. The situation near $(0, 0, 1)$ is more ambiguous since polarized experiments have not yet been performed. A single broad peak is observed. Since it has the same shape at two different equivalent wave-vectors, if it results from two branches they must be very close together in energy. Since the predicted splitting between y and xz modes is larger in this case, due to the increased three-dimensionality, this is difficult to understand. An alternative possibility is that the observed peak only results from the y-branch. Possibly the higher

energy xz branch is too broad to be observable in $RbNiCl_3$. If this is the case then the spectrum is not qualitatively different than that predicted by conventional spin-wave theory. The main quantitative difference is that branch 3 is higher in energy than predicted by that theory. This issue could be resolved by polarized neutron-scattering experiments.

Experments have also been reported on the $s = 5/2$ quasi-one-dimensional antiferromagnet, $CsMnI_3$.[10] This differs in several respects from the other two compounds. Apart from having a larger, half-integer spin, it may also exhibit more Ising anisotropy; the spins on the B and C sub-lattice (see Figure 1) are measured to make an angle of 51^0 with the z-axis rather than 59^0 as in $CsNiCl_3$. It is not clear if the Landau-Ginsburg model is ever applicable in the case of half-integer spin since the zero temperature phase transition may be in a different universality class, even for a cubic lattice. In any event, since the spin is quite large in this case, as is the anisotropy, it seems likely that conventional spin-wave theory would provide an at least qualitatively reliable description. So far only a single peak has been observed near $(0, 0, 1)$. Polarized neutron-scattering experiments are needed to determine if this peak again contains contributions from two branches. The various other branches predicted by anisotropic spin-wave theory have not yet been observed.

III. RENORMALIZATION GROUP ARGUMENTS

In this section we apply renormalization group methods to go beyond the Gaussian approximation to the Landau-Ginsburg model used in Section 2. We use universality arguments to justify the passage from "hard spin" to "soft spin" models. We show that the phase transition as a function of interchain coupling, J', is second order for a bipartite lattice but first order for a stacked triangular lattice. In the former

case we show that the longitudinal mode becomes stable at the critical point. We verify the conclusions in this case by comparing with the large-n limit of the $O(n)$ non-linear σ-model.

It must be emphasized at the outset that we can deduce exact results (subject to generally accepted assumptions) about these problems because of the fact that the phase transition as a function of J', at zero temperature is in the *four-dimensional* universality class. Since this is the upper critical dimension for the phase transition it is Gaussian, up to logarithmic corrections. Consequently, conclusions drawn from a weak-coupling analysis of the Landau-Ginsburg model become exact at the critical point.

We begin by considering the bipartite lattice case. As we approach the critical point we expect the correlation length to diverge, both along the chains and also for interchain correlations. Thus, we may replace the discrete sum over chains in Eq. (2.6) by an integral. Upon rescaling lengths in the basal plane appropriately, we obtain the standard ϕ^4 quantum field theory in $(3+1)$ space-time dimensions with Lagrangian density:

$$\mathcal{L} = (1/2v)(\partial\vec{\phi}/\partial t)^2 - (v/2)(\nabla\vec{\phi})^2 - (\Delta_3^2/2)|\vec{\phi}|^2 - (\lambda/4)|\vec{\phi}|^4 \tag{3.1}$$

Here Δ_3^2 is an effective parameter in this long-wavelength theory which corresponds roughly to $\Delta^2 - 16J'vs$. A crucial point is that this model is Lorentz-invariant due to the second-order time derivitive. [See the appendix for a review of how this second-order term arises.] We expect all breaking of Lorentz-invariance to become irrelevant near the critical point. The Feynman path-integral formulation of the theory is most easily studied by going to imaginary time (ie. Euclidean space): $t \to i\tau$. The Euclidean space Lagrangian density is:

$$\mathcal{L}_E = (1/2)(\nabla_4\vec{\phi})^2 + (\Delta_3^2/2)|\vec{\phi}|^2 + (\lambda/4)|\vec{\phi}|^4. \tag{3.2}$$

Here ∇_4 represent the gradient in the four-dimensional space, and we have absorbed the velocity v into a rescaling of the time co-ordinate. This is precisly the standard classical Landau-Ginsburg Hamiltonian in 4 (space) dimensions which would be used to model a finite-temperature classical magnetic transition. The Feynman path integral corresponds to the usual Boltzmann sum. Thus the fact that the classical system in four dimension is governed by the Gaussian fixed point applies immediately to the quantum system at $T = 0$ in three dimensions. This result is well-known in quantum field theory of course; it is usually referred to as the triviality of ϕ^4 theory.

The renormalization group flows[4] are shown in Figure 11. The critical trajectory separating broken and unbroken symmetry phases flows into $\Delta_3^2 = \lambda = 0$ at long length (or time) scales. This is much different than in lower dimensions. In $4 - \epsilon$ space-time dimensions the Gaussian ($\lambda = 0$) fixed point is unstable and the phase transition is controlled by a fixed point at λ_c of $O(\epsilon)$. In three space-time dimensions λ is expected to be $O(1)$ at the critical point. Consequently the zero-temperature phase transition, as a function of J' is much more trivial than the one that occurs as a function of temperature. In the $T = 0$ case, along the critical trajectory, the effective coupling constant is governed by the β-function:

$$d\lambda/dlnL = -(11/8\pi^2)\lambda^2 + (69/64\pi^4)\lambda^3 + ... \tag{3.3}$$

The solution, at large length scales and small couplings is:

$$\lambda(L) \rightarrow \lambda(L_0)/[1 + (11/8\pi^2)\lambda(L_0)ln(L/L_0)] \tag{3.4}$$

The coupling constant flows to zero logarithmically slowly, at large length scales. Away from the critical point, this decrease of λ ceases at a scale L of order the correlation length. [See Figure 11.] On the ordered side we may estimate this scale as the inverse-size of the order parameter: $L_0/L \propto < \phi >$. Thus we obtain the universal prediction:

$$\lambda(L) \rightarrow 8\pi^2/11|ln < \phi > | \tag{3.5}$$

as $< \phi > \rightarrow 0$. To lowest non-trivial order in λ, the mass of the longitudinal mode, for $\Delta_3^2 < 0$ is given by $\Delta_L^2 = -2\Delta_3^2$, and its decay rate is given by

$$\Gamma_L = \lambda\Delta_L/32\pi \tag{3.6}$$

Thus the width to gap ratio is: $\Gamma_L/\Delta_L = \lambda/32\pi$. The renormalization group prediction can be obtained from this by simply replacing λ by $\lambda(L)$, the effective coupling constant at scale L. (The anomalous dimension factors which normally arise cancel between Δ_L and Λ_L.) Hence:

$$\Gamma_L/\Delta_L \rightarrow \frac{\pi}{44|ln < \phi > |} \tag{3.7}$$

The longitudinal mode becomes infinitely stable at the critical point. We note that $\mathcal{S}^{zz}$ contains a two-magnon continuum starting at zero energy, as well as the longitudinal mode. The strength of this two-magnon contribution vanishes as the critical point is approached. This means that the spin Green's function, expressed as a function of the invariant momentum $p^2 \equiv E^2 - v^2\vec{p}^2$, has both a cut on the positive p^2 axis beginning at $p^2 = 0$ and a pole displaced off the axis at $p^2 \approx \Delta_L^2 + 2i\Delta_L\Gamma$.

As we approach the critical point the intensity of the cut goes to zero and the pole approaches the origin along a trajectory which approaches the real axis. We give an explicit example of this behavior below, using the large-n limit.

So far, we have only discussed the Landau-Ginsburg model in this section. However, by universality, we expect these arguments to be much more general. The Gaussian fixed point is expected to be the universal stable fixed point governing the symmetry-breaking phase transition $SO(3) \rightarrow SO(2)$ in four space-time dimensions. Essentially any model which undergoes such a phase transition is expected to flow to the zero-coupling Landau-Ginsburg fixed point under renormalization. This should be true, for example, of the non-linear σ-model. Formally, this is obtained from the Landau-Ginsburg model by taking $\Delta_3^2 \rightarrow -\infty$ with Δ_3^2/λ held fixed. In this limit $\vec{\phi}^2 = 1$; longitudinal fluctuations have infinite mass. However, if we assume that the renormalization group flows shown in Figure 11 extend all the way to infinity, then we conclude that the non-linear σ-model renormalizes from $\lambda = \infty$ all the way to $\lambda = 0$ at the critical point. This flow is noted schematically in Figure 11. *This implies that the Landau-Ginsburg model should be better than the non-linear σ-model for describing the physics close to the critical point.* We expect that the quantum Heisenberg model, which is the starting point or microscopic model for the study of quantum spin systems, will also be attracted to the Gaussian fixed point.

An instructive illustration of the above discussion is provided by the large-n limits of both Landau-Ginsburg and non-linear σ-models. We briefly review this limit, following the notation and approach of Ref. (11). The starting point is to generalize the 3-component vector, $\vec{\phi}$, to n components, and then let $n \rightarrow \infty$. The four-dimensional Langrangian is written exactly as in Eq. (3.1) except that we replace the coupling constant λ by λ/n in order to have a smooth large-n limit. The non-

linear σ-model is obtained by taking the limit $\Delta_3^2 \to -\infty$ with $< \phi >^2 = -n\Delta_3^2/\lambda \equiv n/g$ held fixed. In this limit longitudinal fluctuations of $\vec{\phi}$ are frozen, at short wavelengths, so $\vec{\phi}$ obeys the constraint $\vec{\phi}^2 = n/g$. The parameter g is the coupling constant of the non-linear σ-model. (The model is often written in terms of a rescaled field, so that the constraint becomes $\vec{\phi}^2 = 1$ and a factor of n/g appears in front of the derivitive terms in the Lagrangian.) A convenient way of dealing with the large-n limit is to introduce an auxiliary field, $\chi(x)$ in terms of which the (Euclidean space) Lagrangian is rewritten:

$$\mathcal{L} = (1/2)\nabla_4\vec{\phi} \cdot \nabla_4\vec{\phi} + n\chi^2/2\lambda + (i\chi/2)(|\vec{\phi}|^2 + n\Delta_3^2/\lambda) \tag{3.8}$$

Upon doing the Gaussian integration over the auxiliary field χ in the path integral, we obtain the original Lagrangian. Note that in the non-linear σ-model limit, the term in $\mathcal{L}$ quadratic in χ vanishes so the effect of the χ integration is to impose the local constraint $\vec{\phi}^2 = -n\Delta_3^2/\lambda$. The next step is to integrate over the fields $\vec{\phi}$ in the path integral. This can be done exactly since they now appear only quadratically in $\mathcal{L}$. Because there are n ϕ fields, the resulting trace-log term has a prefactor, n. In order to study the possibility of spontaneous symmetry breaking in which $< \phi > \neq 0$, it is convenient to integrate only over $n-1$ of the ϕ-fields and leave ϕ_1 in the action so that it may obtain an expectation value. The resulting effective action becomes:

$$S(\phi_1, \chi) = \int d^4x[(1/2)\nabla_4\phi_1 \cdot \nabla_4\phi_1 + n\chi^2/2\lambda + (i\chi/2)(\phi_1^2 + n\Delta_3^2/\lambda)] + [(n-1)/2]tr\ ln[-\partial^2 + i\chi] \tag{3.9}$$

We now look for a saddle-point configuration in which the fields ϕ_1 and χ are constant and expand the functional integral in powers of the fluctuations away

from the saddle-point. It can be easily seen that this gives a series in $1/n$. The saddle-point configuration is of two possible types depending on the values of λ and Δ^2 (or g in the σ-model limit). In the broken-symmetry phase, which we are interested in here, $< \chi >= 0$ and $< \phi_1 > \neq 0$ at the saddle point. The value of $< \phi_1 >$ is determined by setting to zero $\partial S/\partial \chi$. This gives the equation, in the large-n limit:

$$< \phi_1 >^2 = -n\Delta_3^2/\lambda - n \int \frac{d^4k}{(2\pi)^4} \frac{1}{k^2} \tag{3.10}$$

We must impose an ultra-violet cut-off, Λ on the momentum integral (effectively given by the lattice spacing and the exchange energy, J, in the quantum spin problem), so the above integral gives $\Lambda^2/16\pi^2$. We see that a solution exists (ie. the system is in the broken symmetry phase) provided that $-\Delta_3^2/\lambda > \Lambda^2/16\pi^2$ (or $1/g > \Lambda^2/16\pi^2$ in the σ-model limit.) We now expand the action to quadratic order in the fluctuations around the saddle-point, writing $\phi_1 =< \phi > +\phi_L$. The term quadratic in χ involves the integral:

$$B(p)^2 \equiv (1/2) \int \frac{d^4k}{(2\pi)^4} \frac{1}{k^2} \frac{1}{(k+p)^2} \tag{3.11}$$

For momenta much less than the cut-off, $B(p^2) \approx (1/32\pi^2)[1 + ln\Lambda^2/(-p^2)]$. Here we have made the analytic continuation back to real time and $p^2 \equiv E^2 - \vec{p}^2$. Rescaling χ by a factor of $\sqrt{n}$, the quadractic part of the action, written in momentum space, in matrix form, becomes:

$$S = \frac{1}{2} \int \frac{d^4p}{2\pi^4} [\phi_L(p), \chi(p)] \begin{pmatrix} p^2 & i < \phi > \\ -i < \phi > & [1/\lambda + B(p^2)] \end{pmatrix} \begin{pmatrix} \phi_L(-p) \\ \chi(-p) \end{pmatrix} \tag{3.12}$$

Here ($\phi >$ is given by Eq. (3.10). The propagator (ie. the Fourier transform of the

time-ordered Green's function) is given by the inverse of the matrix appearing in S. Thus in particular the ϕ_L propagator is given by:

$$D(p^2) \equiv < \phi_L \phi_L > (p) = \frac{i\{1/\lambda + (1/32\pi^2)[1 + ln(\Lambda^2/(-p^2)]\}}{p^2\{1/\lambda + (1/32\pi^2)[1 + ln\Lambda^2/(-p^2)]\} - < \phi >^2} \tag{3.13}$$

In the non-linear σ-model limit this takes the simpler form:

$$D(p^2) \equiv < \phi_L \phi_L > (p) = \frac{(i/32\pi^2)[1 + ln\Lambda^2/(-p^2)]}{p^2(1/32\pi^2)[1 + ln\Lambda^2/(-p^2)] - < \phi >^2} \tag{3.14}$$

The real part of D gives the 11 component of the neutron scattering cross-section, $< \mathcal{S}^1\mathcal{S}^1 >$. This illustrates all the general features expected from the renormalization group arguments. First focus on the weak-coupling limit of the Landau-Ginsburg model, assuming $1/\lambda >> (1/32\pi^2)ln(\Lambda^2/ < \phi >^2)$. We see that $D(p^2)$ has a pole given approximately by $p^2 \approx \lambda < \phi >^2 \approx \Delta_L^2$. The pole is actually displaced slightly off the real axis since $ln(-p^2)$ has an imaginary part for positive p^2. Thus, at the pole,

$$Im\ p^2 \approx \lambda\Delta_L^2/32\pi \tag{3.15}$$

The position of the pole can be written as $\Delta_L^2 + 2i\Delta_L\Gamma$, where Γ is the decay rate. Thus we find:

$$\Gamma \approx \lambda\Delta_L/64\pi \tag{3.16}$$

This agrees with Eq. (3.6) up to a factor of 2 which arises from rescaling λ and making the large-n approximation. A better approximation to Γ is obtained by making the replacement:

$$1/\lambda \rightarrow 1/\lambda_{eff} \equiv 1/\lambda + (1/32\pi^2) ln\Lambda^2/\Delta_L^2 \tag{3.17}$$

in Eq. (3.16), with Δ_L determined by:

$$< \phi >^2 = \Delta_L^2[1/\lambda + (1/32\pi^2) ln(\Lambda^2/\Delta_L^2)] \tag{3.18}$$

We see that Eq. (3.16) will be approximately correct with these replacements whenever $\lambda_{eff} << 32\pi$.

λ_{eff} is just the effective coupling constant determined from the renormalization group (in the large-n limit) evaluated at the scale Δ_L. We see that, for $\Delta_L^2 << \Lambda^2$ the effective coupling becomes small, even if the bare coupling is not. In fact this remains true even in the non-linear σ-model limit, where the bare coupling is infinite. In this case Eq.(3.17) reduces to:

$$1/\lambda_{eff} \equiv (1/32\pi^2) ln\Lambda^2/\Delta_L^2 \tag{3.19}$$

Thus we see explicitly, in the large-n limit, that the non-linear σ-model becomes equivalent to the Landau-Ginsburg model with a small coupling constant, near the critical point where $< \phi >^2$ and Δ_L^2 vanish. Up to a $ln\ ln$ term we may replace Δ_L^2 by $< \phi >^2$ inside the logarithm.

We also see from Eq. (3.13) and (3.14) that, for $|p^2| << \Delta_L^2$, the propagator has a cut:

$$D(p^2) \rightarrow -\frac{i}{32\pi^2 < \phi >^2} ln\Lambda^2/(-p^2) \tag{3.20}$$

This arises from the two-Goldstone boson intermediate state. Thus the real part

of D, which gives the neutron-scattering cross-section, has a constant part at small positive p^2 coming from the two-magnon contribution and then a resonance at $p^2 \approx -\Delta_L^2$ from the longitudinal mode. As $< \phi >^2 \rightarrow 0$ the resonance moves down to $p^2 = 0$, and right at the critical point the propagator reduces to $D(p^2) \rightarrow i/(p^2 + i\epsilon)$; the real part collapses to a δ-function at $p^2 = 0$. Close to the critical point most of the integrated intensity comes from the resonance, not the cut.

We now turn to the triangular lattice case. It is important to realize that the order-disorder phase transition is in a different universality class than in the bipartite case. This follows from the fact that there is an unbroken $SO(2)$ symmetry in the Néel state on a bipartite lattice (rotation of the spins about the unique ordering axis) but not in the triangular lattice where the ordered state involves three different axes making angles of $2\pi/3$ with respect to each other, as shown in Figure 1. Now taking the continuum limit of the three-dimensional Landau-Ginsburg model, we must introduce three fields, $\vec{\phi}_i$, $i = 1, 2, 3$ labelling the three inequivalent sub-lattices in the basal plane. The quadratic part of the potential energy is of the form:

$$V_2 = \sum_{i=1}^{3} (\Delta^2/2v)|\vec{\phi}_i|^2 + 12J's(\vec{\phi}_1 \cdot \vec{\phi}_2 + \vec{\phi}_2 \cdot \vec{\phi}_3 + \vec{\phi}_3 \cdot \vec{\phi}_1) \tag{3.21}$$

It is now convenient to change variables to:

$$\vec{\phi}_a = (2\vec{\phi}_1 - \vec{\phi}_2 - \vec{\phi}_3)/\sqrt{6} \tag{3.22}$$

$$\vec{\phi}_b = (\vec{\phi}_2 - \vec{\phi}_3)/\sqrt{2} \tag{3.23}$$

$$\vec{\phi}_c = (\vec{\phi}_1 + \vec{\phi}_2 + \vec{\phi}_3)/\sqrt{3} \tag{3.24}$$

This diagonalizes the quadratic terms giving:

$$V_2 \rightarrow (1/2)(\Delta^2/v - 12J's)(|\vec{\phi}_a|^2 + |\vec{\phi}_b|^2) + (1/2)(\Delta^2/v + 24J's)|\vec{\phi}_c|^2 \tag{3.25}$$

We see that as we increase J', the a and b modes eventually become gapless whereas the c mode gets a larger gap. $\vec{\phi}_c$ is the *ferromagnetic* order parameter; its gap vanishes if J' is sufficiently large and *negative*. Since we are interested in the anti-ferromagnetic case, we may simply drop the massive mode, $\vec{\phi}_c$, from the low-energy theory. The two remaining modes, $\vec{\phi}_a$ and $\vec{\phi}_b$, can be combined into a complex three-vector field:

$$\vec{\Phi} \equiv (\vec{\phi}_a + i\vec{\phi}_b)/\sqrt{2} \tag{3.26}$$

The original spin operators are related to $\vec{\Phi}$ by:

$$\vec{S}_i \propto Re\ (\vec{\Phi} e^{i\vec{Q}_2 \cdot \vec{x}_i}) \tag{3.27}$$

where $\vec{Q}_2$ is the ordering wave-vector projected onto the basal plane, given in Eq. (2.28). The complete Landau-Ginsburg model may be rewritten in terms of $\vec{\Phi}$ (after eliminating $\vec{\phi}_c$) as:

$$\mathcal{L} = \nabla_4 \vec{\Phi}^* \cdot \nabla_4 \vec{\Phi} + \Delta_3^2 \vec{\Phi}^* \cdot \vec{\Phi} + (\lambda_1/4)(\vec{\Phi}^* \cdot \vec{\Phi})^2 + (\lambda_2/4)(\vec{\Phi} \cdot \vec{\Phi})(\vec{\Phi}^* \cdot \vec{\Phi}^*) \tag{3.28}$$

Here Δ_3^2 is an effective renormalized gap parameter, as before. The two coupling constants, λ_1 and λ_2 are determined by the original single coupling constant, λ. To lowest order in λ, they have the values, $\lambda_1 = 4\lambda/3$, $\lambda_2 = 2\lambda/3$. They are both positive, resulting in an ordered state with $Re\ \vec{\Phi} \perp Im\ \vec{\Phi}$. This gives the expected $2\pi/3$ structure, from Eq. (3.27). Higher order corrections to the Lagrangian are obtained from integrating out $\vec{\phi}_c$. However, these only produce corrections to Δ_3^2, λ_1 and λ_2 together with terms of higher order in derivitives or in powers of the

fields. This follows from the discrete symmetry: $\vec{\phi}_1 \rightarrow \vec{\phi}_2 \rightarrow \vec{\phi}_3 \rightarrow \vec{\phi}_1$, which corresponds to $\vec{\Phi} \rightarrow e^{-2\pi i/3}\vec{\Phi}$. This symmetry forbids any other non-derivitive quadratic or quartic terms. [Note that this Z_3 symmetry is actually enlarged to a $U(1)$ symmetry in the Landau-Ginsburg model. Only by keeping sixth order terms in $\mathcal{L}$ is the symmetry reduced to the Z_3 subgroup.] Thus the effective Landau-Ginsburg Lagrangian density must have the form of Eq. (3.28) with some effective parameters, Δ_3^2, λ_1, λ_2. The β-function has been calculated for this model:[5]

$$d\lambda_1/dlnL = -(1/16\pi^2)(7\lambda_1^2 + 4\lambda_1\lambda_2 + 4\lambda_2^2) + O(\lambda^3) \tag{3.29}$$

$$d\lambda_2/dlnL = -(1/16\pi^2)(6\lambda_1\lambda_2 + 3\lambda_2^2) + O(\lambda^3) \tag{3.30}$$

The resulting renormalization group flows are shown in Figure 12. Note that only the line $\lambda_2 = 0$ flows to the origin in coupling constant space. Otherwise all trajectories flow to $\lambda_1 = -\infty$, $\lambda_2 = \pm\infty$. Thus we see that the Gaussian fixed point is not stable, for this phase transition, in four space-time dimensions. The usual interpretation of this kind of renormalization group flow is that the phase transition is driven first-order by fluctuations. This is signified by the negative value of λ_1 upon renormalization. Including positive $|\vec{\phi}|^6$ terms for stability, we find a first order phase transition in Landau theory. There has been some controversy lately over the corresponding phase transition *in three dimensions*, which would correspond to the finite-temperature transition in $CsNiCl_3$. It may be first or second order. However, in four dimensions there seems to be no question; the Gaussian fixed point is unstable so the transition is expected to be first order.

What does this imply about the longitudinal mode? We should expect that as the interchain coupling, J', is decreased in the ordered phase, the sub-lattice magnetization will decrease smoothly for a while, but eventually will make a discontinuous

drop to zero at J'_c. Correspondingly, we expect that the mass of the longitudinal mode will decrease smoothly before dropping abruptly to zero. It also seems plausible that the effective coupling constants will at first decrease, before the first order transition point is reached. Thus we might expect the width to mass ratio of the longitudinal mode to decrease with increasing J'. Of course, this ratio will never reach zero; before this happens the transition to the disordered phase will occur. The value of this ratio at the first-order transition point, J'_c, is non-universal. Whether or not the longitudinal mode will ever be observable in a stacked triangular system is an empirical question. As we have tried to argue in Section II, the experimental evidence in $CsNiCl_3$ suggests that it has been.

IV. NEUTRON-SCATTERING IN A FINITE FIELD

In this section we consider the effect of a magnetic field on the magnon dispersion relation in the ordered phase, for the case of a stacked triangular lattice antiferromagnet.[12] We first present the result of conventional spin-wave theory. (As far as we know, this simple result has not been published before in its entirety.) We then present the analagous result using the Landau-Ginsburg model; ie. including the longitudinal mode. Some comparison is then made with finite-field neutron-scattering experiments on $CsNiCl_3$[6]. Finite field effects in the disordered phase of Haldane gap antiferromagnets have been discussed elsewhere.[13] In the case under consideration here, where crystal field (or exchange) anistropy can be ignored and the Zeeman energy is smaller than the Haldane gap, the result is extremely simple. The Haldane triplet simply undergoes a Zeeman splitting with energies Δ, $\Delta \pm g\mu_B h$, where h is the magnetic field. As we have emphasized above, in the Landau-Ginsburg model we go smoothly from disordered to ordered phases by varying the interchain coupling. (However the transition is driven first order by

fluctuations in the stacked triangular lattice case.) This remains true when a magnetic field is included, with the field lowering J'_c. Thus, in weak fields, for J' only slightly bigger than J'_c the Landau-Ginsburg model predicts behavior much different than does conventional spin-wave theory. This behavior goes over smoothly into the simple Zeeman-splitting of the disordered phase as $J' \to J'_c$. The finite-field experiments provide evidence for such an effect in $CsNiCl_3$.

Following the experimental set-up, the spins are ordered in the xz plane (at $h \to 0$), as in Figure 1 and the magnetic field, h, is applied along the y-axis. We first consider the classical problem, regarding each spin as a classical vector, of length s. This gives the starting point for standard spin-wave theory. (Note that this is not quite the same as the classical limit of the Landau-Ginsburg model because that model is developped in terms of the *staggered* magnetization.) Classically, each spin cants in the y-direction by the angle θ, without changing its orientation in the xz-plane. The classical energy per spin is:

$$E/N = -2Js^2 cos2\theta - g\mu_B hs \sin\theta + 6J's^2 \left(1 - \frac{3cos^2\theta}{2}\right)$$

Minimizing E with respect to θ gives:

$$\sin\theta = \frac{g\mu_B h}{s(8J + 18J')} \tag{4.1}$$

We note that for $CsNiCl_3$, $J/h_P \approx .345THz$, so, for the maximum field of $6T$ used in the experiment, $sin\theta \approx .06$.

To calculate the dispersion relation using conventional spin-wave theory, we expand around the classical groundstate, calculated above, to quadratic order in magnon creation and annihilation operators. The calculation can be considerably simplified by the observation that, as in the zero-field case, the classical groundstate

is invariant under translation by one site together with a rotation by $2\pi/3$ in the xz-plane. (This symmetry is *not* destroyed by canting.) For zero canting, the spin operators on the A sublattice (see Figure 1) are expanded as:

$$\vec{S}^0 = \left(\sqrt{\frac{s}{2}}(a^\dagger + a), i\sqrt{\frac{s}{2}}(a^\dagger - a), s - a^\dagger a\right) \tag{4.2}$$

This is the correct representation when the spin points in the z-direction in the classical approximation. Here a ($a^\dagger$) annihilates (creates) a boson. To obtain the correct representation on the six different sub-lattices, in the presence of canting, we simply rotate $\vec{S}^0$ by the rotation matrix which produces the correct classical state from the one where the spin points in the z direction. The needed rotation matrices are: $\mathbf{R}_1$, the cant (rotation by $-\theta$ about the x-axis), $\mathbf{R}_2$ a rotation by $-\frac{2\pi}{3}$ about the y axis, and $\mathbf{R}_3$ a rotation by π about the y axis. The needed representation on the six different sublattices, shown in Figure 1 is:

$$\vec{S}_A = \mathbf{R}_1 \vec{S}_1^0$$

$$\vec{S}_B = \mathbf{R}_2 \vec{S}_A$$

$$\vec{S}_C = \mathbf{R}_2^2 \vec{S}_A$$

$$\vec{S}_D = \mathbf{R}_3 \vec{S}_A$$

$$\vec{S}_E = \mathbf{R}_3 \vec{S}_B$$

$$\vec{S}_F = \mathbf{R}_3 \vec{S}_C$$

The Hamiltonian may now be written in the fully translationally invariant form:

$$H = 2\sum_{j=1}^{N}\left(J\,\vec{S}^0_{1,\vec{x}_j}\cdot\mathbf{B}\vec{S}^0_{1,\vec{x}_j+\vec{\delta}_4} + J'\sum_{l=1}^{3}\vec{S}^0_{1,\vec{x}_j}\cdot\mathbf{A}\vec{S}^0_{1,\vec{x}_j+\vec{\delta}_l} - g\mu_B h S_{\vec{x}_j,y}\right) \tag{4.3}$$

where the $\vec{\delta}_i$'s are the lattice vectors defined in Eq. (2.22) for $i = 1, 2, 3$ and $\vec{\delta}_4 \equiv \vec{a}_3$, defined in Eq. (2.21). $\mathbf{A}$ and $\mathbf{B}$ are real matrices.

$$\mathbf{A} = \mathbf{R}_1^T \mathbf{R}_2 \mathbf{R}_1 = \begin{pmatrix} -\frac{1}{2} & -\frac{\sqrt{3}\sin\theta}{2} & \frac{\sqrt{3}cos\theta}{2} \\ \frac{\sqrt{3}\sin\theta}{2} & cos^2\theta - \frac{\sin^2\theta}{2} & \frac{3\sin\theta\, cos\theta}{2} \\ -\frac{\sqrt{3}cos\theta}{2} & \frac{3\sin\theta\, cos\theta}{2} & \sin^2\theta - \frac{cos^2\theta}{2} \end{pmatrix}$$

$$\mathbf{B} = \mathbf{R}_1^T \mathbf{R}_3 \mathbf{R}_1 = \begin{pmatrix} -1 & 0 & 0 \\ 0 & cos2\theta & \sin 2\theta \\ 0 & \sin 2\theta & -cos2\theta \end{pmatrix}$$

Note that, while $\mathbf{B}$ is symmetric, $\mathbf{A}$ is not. Thus the Hamiltonian of Eq. (4.3) is not invariant under reflections in the basal plane. We now Fourier transform. Since the Hamiltonian of Eq. (4.3) has the full lattice translation symmetry, we may introduce Fourier modes in the full paramagnetic Brillouin zone. The quadratic terms in H become:

$$\begin{aligned} H_2 = \sum_{k=1}^{N} \Big\{ \Big[& 4Js\cos 2\theta - 4Js\sin^2\theta\, \cos(cQ_z/2) + g\mu_B h \sin\theta + 12J's\left(\frac{3\cos^2\theta}{2} - 1\right) \\ & + J's f(\vec{Q}_\perp)\left(1 - 3\sin^2\theta\right)\Big] a^\dagger_{\vec{Q}} a_{\vec{Q}} \\ & - \left[2Js\cos^2\theta\, \cos(cQ_z/2) + \frac{3}{2}J's\cos^2\theta\, f(\vec{Q}_\perp)\right]\left(a^\dagger_{\vec{Q}} a^\dagger_{-\vec{Q}} + a_{\vec{Q}} a_{-\vec{Q}}\right)\Big\} \end{aligned} \tag{4.4}$$

$f(\vec{Q}_\perp)$ is defined in Eq. (2.40). We now diagonalize H_2 by a Bogliubov transformation, giving the dispersion relation:

$$\begin{aligned} E^2(\vec{Q}) = & \left[4Js\left(1 - \sin^2\theta\, cos(cQ_z/2)\right) + J's\left(6 + f(\vec{Q}_\perp) - 3\sin^2\theta f(\vec{Q}_\perp)\right)\right]^2 \\ & - \left[4Js\ cos^2\theta\, cos(cQ_z/2) + 3J's cos^2\theta\, f(\vec{Q}_\perp)\right]^2 \end{aligned} \tag{4.5}$$

Defining $E_0(\vec{Q})$ to be the zero field energy:

$$E_0^2(\vec{Q}) = \left[4Js + J's\left(6 + f(\vec{Q}_\perp)\right)\right]^2 - \left[4Js\ cos(cQ_z/2) + 3J's f(\vec{Q}_\perp)\right]^2$$

this can be conveniently rewritten as:

$$E(\vec{Q}) = \sqrt{E_0^2(\vec{Q}) + c(\vec{Q})s^2 \sin^2\theta} \tag{4.6}$$

where

$$c(\vec{Q}) \equiv 32J^2 \left(cos^2(cQ_z/2) - cos(cQ_z/2)\right) + 8JJ' \left(5cos(cQ_z/2)\, f(\vec{Q}_\perp) - 3f(\vec{Q}_\perp) - 6cos(cQ_z/2)\right)$$
$$+12J'^2 \left(f(\vec{Q}_\perp)^2 - 3f(\vec{Q}_\perp)\right) \tag{4.7}$$

Taking into account the rotating reference frame implicit in the definition of the a_j's, we find a single branch of magnons with y-polarization and two with xz-polarization:

$$E_y(\vec{Q}) = E(\vec{Q}) \tag{4.8}$$

$$E_{xz\pm}(\vec{Q}) = E(\vec{Q} \pm \vec{Q}_0) \tag{4.9}$$

Note that, in zero field, $E_0(\vec{Q})$ vanishes at $\vec{Q} = 0$ and also at the twelve corners of the paramagnetic Brillouin zone. (See Figure 3.) Consequently, E_y and $E_{xz\pm}$ each vanish at one inequivalent wave-vector in the antiferromagnetic zone. These are the three Goldstone modes corresponding to the complete breaking of rotational symmetry. E_y and E_{xz-} vanish in zero field at $(Q_1, Q_2, Q_3) = (1/3, 1/3, 1)$, the ordering wave-vector. [See figures 6a and 8.] At non-zero field, $E(\vec{Q})$ only vanishes at $\vec{Q} = 0$ since $c(\vec{Q})$ vanishes at $\vec{Q} = 0$ but not at the corners of the parmagnetic zone. Thus only E_{xz-} vanishes at the ordering wave-vector. This corresponds to the fact that, classically, rotations of the canted spin configuration in the xz-plane costs zero energy but any rotation involving a change in the y-components of the spins costs energy. In fact, $c(\vec{Q})$ is relatively small, of $O(J'J)$ whenever $Q_z = 0$.

Consequently the change in the energies of the xz modes for fields less than $6T$ in $CsNiCl_3$ is negligible for all wave-vectors considered in this paper. Only the y-mode is significantly effected by a $6T$ field, and that effect is itself rather small except near the ordering wave-vector. The y-mode dispersion relation at fields of 0 and $6T$ is shown in Figure 13. We do not show the xz-dispersion relation at $6T$ because, to the naked eye, it is indistinguishible from the zero field result in Figure 8.

Note that this field-dependence, predicted by spin-wave theory, is completely different than that which occurs in the disordered phase. In this case, for the field applied along the y-axis, the y-mode, which has $\mathcal{S}^y = 0$ is completely unaffected by the field and the xz-modes, which have $\mathcal{S}^y = \pm 1$ have a Zeeman splitting $\pm g\mu_B h$.

Let us now consider the experimental field dependence at $(0,0,1)$, $(.1,.1,1)$ and $(.39,.39,1)$ shown by the circles in Figures 14-19. Note that the y-mode is quite weakly affected by the field, and its field-dependence is quite well-predicted by conventional spin-wave theory. However, the xz-mode shows a stronger field-dependence than the y-mode and is not at all described by conventional spin-wave theory which predicts essentially field-independent frequencies. Remarkably, the experimental behavior is much better fit by the disordered phase behavior than by spin-wave theory, despite the fact that the system is in the ordered phase. Since the Landau-Ginsburg model interpolates smoothly between spin-wave theory and the disordered phase behavior, we might expect it to give a good description of this behavior.

We now consider magnetic field-dependence in the Landau-Ginsburg model. The Lagrangian is obtained from Eq. (2.3) by the replacement:

$$\partial\vec{\phi}/\partial t \rightarrow \partial\vec{\phi}/\partial t + g\mu_B\vec{h} \times \vec{\phi} \tag{4.10}$$

We must first recalculate $< \vec{\phi} >$ in the presence of the field. Assuming a uniform value of $\vec{\phi}$ on each sub-lattice of chains, we obtain the potential energy per antiferromagnetic unit cell:

$$V = \sum_{i=1}^{3} \left[\frac{\Delta^2}{2v} \phi_i^2 + (\lambda/4)\vec{\phi}_i^4 - \frac{(g\mu_B \vec{h} \times \vec{\phi}_i)^2}{2v} \right] + (4J's/c)[\vec{\phi}_1 \cdot \vec{\phi}_2 + \vec{\phi}_2 \cdot \vec{\phi}_3 + \vec{\phi}_3 \cdot \vec{\phi}_1] \tag{4.11}$$

Choosing the magnetic field to lie along the y-axis, we see that the minimizing configuration for the $\vec{\phi}_i$'s is still the $2\pi/3$ structure in the xz-plane, but with a different magnitude of $\vec{\phi}$. This might seem to contradict the classical result discussed above which involved a canting of the spins in the y-direction. However, there is no contradiction because this canting is *uniform* along the chains. Thus it does not show up in $\vec{\phi}$, the staggered magnetization but only in

$$\vec{l} \equiv (1/v)\vec{\phi} \times (\partial\vec{\phi}/\partial t + g\mu_B \vec{h} \times \vec{\phi}) = (g\mu_B/v) < \phi >^2 \vec{h} \tag{4.12}$$

Assuming the $2\pi/3$ structure, the potential energy per chain per unit length becomes:

$$V \rightarrow \{[\Delta^2 - (g\mu_B h)^2]/2v - 12J's/c\}\phi^2 + \lambda\phi^4/4 \tag{4.13}$$

Note that the applied field decreases the effective Δ^2 and favours the ordered phase. The sub-lattice magnetization is given by:

$$\phi^2 = [(g\mu_B h)^2 + 24J'sv/c - \Delta^2]/\lambda v \tag{4.14}$$

This sensitive dependence of the sub-lattice magnetization on external field leads to a strong field-dependence of magnon energies.

To calculate the dispersion relation, we introduce the same rotating co-ordinate system and modes as in Eqs. (2.33,2.34) and expand the Lagrangian to quadratic order. The terms quadratic in the y-mode, ϕ_2 are exactly the same as previously, Eq. (2.35), except that the value of $< \phi >$ has changed, now being given by Eq. (4.14). On the other hand, the terms quadratic in transverse and longitudinal xz-modes, ϕ_1 and ϕ_L are the same as previously, Eq. (2.37) (expressed in terms of the new value of $< \phi >$) plus the additional terms:

$$\delta\mathcal{L}_{xz} = \sum_i \left[\frac{g\mu_B h}{v} \left(\frac{\partial \phi_{1i}}{\partial t} \phi_{Li} - \frac{\partial \phi_{Li}}{\partial t} \phi_{1i} \right) + \frac{(g\mu_B h)^2 (\phi_{1i}^2 + \phi_{Li}^2)}{2v} \right] \tag{4.15}$$

At this point we Fourier transform with respect to space and time. The energy of the y-mode is given by:

$$E_2(Q_z - 2\pi/c, \vec{Q}_\perp)^2 = (vQ_z)^2 + (8J'vs/c)[3 + 2f(\vec{Q}_\perp)] + (g\mu_B h)^2 \tag{4.16}$$

This is the same result as obtained from conventional spin-wave theory, Eq.(4.6), for small $Q_z - 2\pi/c$ and J'. The agreement with experiment, shown in Figures 14-16, is quite good. The classical equations of motion mix the transverse and longitudinal xz-modes as before. The classical frequencies are now given by the vanishing determinant condition:

$$\begin{vmatrix} -E^2 + v^2Q_z^2 + 8J'sv/(3-f)c & -2ig\mu_B hE - 8\sqrt{3}iJ'sv\tilde{f}/c \\ 2ig\mu_B hE + 8\sqrt{3}iJ'sv\tilde{f}/c & -E^2 + v^2Q_z^2 + 8J'sv(3-f)/c + \Delta_L^2 + 2(g\mu_B h)^2 \end{vmatrix} = 0 \tag{4.17}$$

This gives a quartic equation in E with four real solutions of both signs. Since $\tilde{f}(-\vec{Q}_\perp) = -\tilde{f}(\vec{Q}_\perp)$, the classical solutions at wave-vector $-\vec{Q}$ are -1 times the

solutions at wave-vector $\vec{Q}$. At the quantum mechanical level, it can be seen that the magnon energies are given by the absolute values of all four classical frequencies, at each wave-vector. The doubling of the number of solutions occurs because the modes at $\vec{Q}$ and $-\vec{Q}$ are mixed. The same wave-vector shift occurs, due to the rotating reference frame as at zero field. Thus there is a single y-mode and, in general, eight xz-modes given by the absolute value of the four solutions of Eq. (4.17) shifted in wave-vector by $\pm\vec{Q}_2$, defined in Eq. (2.28). The xz-frequencies are quite strongly field dependent, due to the field-dependence of $< \phi >$, unlike in conventional spin-wave theory where the field dependence of xz-modes is minute.

The field dependence at wave-vector $(0, 0, 1)$ of the xz-modes is shown in Figure 17. There are only four independent xz branches at this wave-vector. They display behavior reminiscent of Zeeman splitting, as expected, and as observed experimentally. There is some experimental evidence that the single zero-field xz peak is actually split into two with frequencies of about $.42THz$ and $.58THz$. However, due to the low beam intensity in this polarized inelastic neutron scattering experiment, the apparent double peak structure may not be statistically significant. [See Figure 3a of Ref. (8)]. Higher-intensity experiments are needed to resolve this issue. If this splitting is really present, it is probably a result of crystal-field anistropy. Such anistropy can be included in the Landau-Ginsburg model. We expect it to split the upper zero field xz peak into two components. [It also mixes xz and y modes.] We also show the experimental results and theoretical predictions for xz-polarization at wave-vectors $(.1, .1, 1)$ and $(.39, .39, 1)$, in Figures 18 and 19. The non-zero field-dependence of xz-polarized branches disagrees badly with conventional spin-wave theory which predicts an essentially field-independent spectrum given in Figure 8. It is more difficult to say how well it agrees with the Landau-Ginsburg model because we have not yet calculated the intensity or width of the branches at finite

field and because of the low intensity and resolution of the experiments. At $(0,0,1)$ and $(.1,.1,1)$ we expect that lower branches to be of very low intensity at small fields. The Zeeman-like behavior of the upper branches is in at least rough agreement with experiment. Note that at $(.39,.39,1)$, near the ordering wave-vector, the lowest, Goldstone, xz -branch is essentially field-independent, whereas the next lowest branch is split into two by the field.

V. CONCLUSIONS

We may summarize the agreement between theory and experiment as follows. In $CsNiCl_3$, the y-polarized spin-wave spectrum is in good agreement with both theories, which make essentially the same prediction. The xz-polarized spin-wave spectrum disagrees badly with conventional spin-wave theory. In particular we have identified two qualitative features which are missed by this theory: the large ratio of frequencies of the upper mode at $(0,0,1)$ and $(1/3,1/3,1)$ and the strong field-dependence. It is more difficult to estimate the agreement between the Landau-Ginsburg model and experiment for xz-polarized modes. Certain qualitative features are well-explained: the existence of a mode near $(0,0,1)$ which is nearly degenerate with the y-mode and about $2\frac{1}{2}$ times higher than the upper mode at $(1/3,1/3,1)$; strong field-dependence which is Zeeman-like near $(0,0,1)$. The most serious discrepency is probably the none-observation, near $(1/3,1/3,1)$, of xz-branch number 2, shown in Figure 6b, predicted at a frequency of $.28THz$ and an intensity of about 1/3 that of branch number 3 at $.18THz$. High intensity and resolution experiments have so far failed to discover this mode.[14] However, we can argue with some confidence that it must be there since it is the continuation of the upper branch which *is observed* near $(0,0,1)$. It seems quite likely that its energy is renormalized downward so that it cannot be resolved from branch 3, near

$(1/3, 1/3, 1)$. This hypothesis could be checked by measuring intensities. Another fact to keep in mind is that the upper branches are in general of finite width. These widths have so far not been calculated; in particular we do not know their wave-vector dependences. Possibly the second branch becomes unobservably broad near $(1/3, 1/3, 1)$.

The number of so far unobserved modes becomes much higher at finite field. Thus higher intensity and resolution finite-field experiments may provide a more definitive test of the Landau-Ginsburg model.

As we have emphasized, the spin-wave spectrum of the Landau-Ginsburg model goes over smoothly from the ordered to disordered phase (ignoring fluctuation effects which drive the transition first-order for a stacked triangular lattice.) Thus certain features of the experimental data, taken in the ordered phase, which are reminiscent of the behavior of the disordered phase, are explained *naturally* by the Landau-Ginsburg model. These features include the fact that the xz-modes are nearly degenerate with the y-mode near $(0, 0, 1)$ and the fact that these three modes exhibit a Zeeman-like field-dependence. These features are approximately reproduced by the Landau-Ginsburg model with the choice of parameters we have made. There is some indication that $CsNiCl_3$ is exhibiting behavior near $(0, 0, 1)$ which is even more like the disordered phase than that of the Landau-Ginsburg model with these parameters. It is quite possible that higher-order corrections to the model might reproduce this; ie. these might give an effective Δ_L which depends on wave-vector and might by smaller near $(0, 0, 1)$ than near the ordering wave-vector.

A major experimental issue which needs to be resolved is whether the xz-mode at $(0, 0, 1)$ is split into two components even in zero field. The experimental situation presently seems ambiguous. If so, this presumably represents an effect of the Ising-anisotropy.

The situation is $RbNiCl_3$ remains more ambiguous pending polarized neutron-scattering experiments. We do not know whether a portion of branch 2 lies inside the peak observed at $(0,0,1)$. It is possible that this peak contains only the y-mode and that branches 1 and 2 are at higher energy and may be too broad to be observable.

Another type of theoretical prediction that we have made involves the dependence on interchain coupling. We have predicted a first-order transition for a stacked triangular lattice but second-order for a tetragonal lattice. If a material could be found with an interchain to intrachain coupling ratio very close to the critical value, then it might be possible to study the transition by applying pressure to the sample. One could search for such a material by looking for ordered systems with very small antiferromagnetic moments. We note that, in the triangular case where the transition is first order, the moment would decrease, upon decreasing the ratio, to some limiting non-zero value, before dropping discontinuously to zero. Since this limiting value is not known, it is difficult to estimate how close $CsNiCl_3$ is to the phase transition.

We would like to thank Dan Arovas, Bill Buyers, Matthew Fisher, K. Kakurai, Lon Rosen, Michael Steiner and Zin Tun for useful questions, discussions and suggestions.

APPENDIX A: FORM OF THE LAGRANGIAN

An alternative Lagrangian was proposed recently[8] for quasi-one-dimensional antiferromagnets which also contains longitudinal fluctuations, but gives a rather different spin-wave spectrum. The purpose of this appendix is to compare the two approaches and justify the form of the Lagrangian used here.

The path-integral formulation of a single quantum spin is written in terms of

a unit vector, $\hat{S}(t)$ with an action $\mathcal{S} = sA[\hat{S}(t)] - \int dt H[s\hat{S}(t)]$, where A is the oriented area swept out on the unit sphere by the closed path $\hat{S}(t)$, and $H(s\hat{S})$ is the Hamiltonian.[15] [See Figure 20.] There is a 4π ambiguity in the choice of area, A, but the weight, $e^{i\mathcal{S}}$ in the path-integral is single-valued since s must be an integer or half-integer. The equations of motion are derived by varying the action with respect to an infinitesimal change in the path $\hat{S}(t) \to \hat{S}(t) + \delta\hat{S}(t)$. Using [See Figure 21.]:

$$\delta A = \int dt \delta\hat{S} \cdot [\hat{S} \times \partial\hat{S}/\partial t] \tag{A1}$$

we obtain the Euler-Lagrange equation:

$$s\partial\hat{S}(t)/\partial t = -\hat{S}(t) \times \partial H/\partial\hat{S}(t) \tag{A2}$$

For a lattice of coupled quantum spins with Hamiltonian of the general form:

$$H = s^2 \sum_{i,j} J_{ij} \hat{S}_i \cdot \hat{S}_j \tag{A3}$$

this gives the *first order* classical equation:

$$\partial\hat{S}_i/\partial t = -s \sum_j J_{ij} \hat{S}_i \times \hat{S}_j \tag{A4}$$

Note that this is the classical torque equation. The continuum limit is obtained, for an antiferromagnet, by keeping only long-wavelength fluctuations of the uniform and staggered magnetisation density, $\vec{l}$ and $s\vec{\phi}$ respectively. ie. we approximate:

$$s\hat{S}_i \approx \vec{l}(\vec{x}_i) + (-1)^i s\vec{\phi}(\vec{x}_i) \tag{A5}$$

where we obtain a plus or minus sign for the two sub-lattices, and we have again set the lattice spacing to one. For a stacked triangular lattice i labels distance along the chain. Note that $\int dx\vec{l}(\vec{x})$ is the total conserved spin and $s\vec{\phi}$ is the Néel order parameter. In the large-s limit, we expect $\vec{l}$ and $\vec{\phi}$ to both be of O(1). Assuming that $\vec{l}$ and $\vec{\phi}$ vary slowly, the unit-vector constraint on $\hat{S}_i$, becomes:

$$\vec{\phi}^2 = 1 - \vec{l}^2/s^2 \approx 1$$
$$\vec{\phi}\cdot\vec{l} = 0 \tag{6}$$

We substitute this form, Equation (A5) into the action, assuming that both fields, $\vec{l}$ and $\vec{\phi}$ vary slowly over one lattice spacing. Noting that $A[\hat{S}(t)]$ is odd under $\hat{S}(t) \rightarrow -\hat{S}(t)$, we see that the leading term cancels between neighboring sites. There is a correction, of $O(1/s)$ which couples $\vec{l}$ and $\vec{\phi}$:

$$\delta A = (1/s)\int dt\vec{l}\cdot[\vec{\phi}\times\partial\vec{\phi}/\partial t] \tag{A7}$$

In general, it is also important to keep the the other correction which is a triple product of $\vec{\phi}$, $\partial\vec{\phi}/\partial t$ and $\partial\vec{\phi}/\partial x$. This gives the topological term in the non-linear σ-model in $(1+1)$ dimensions. However, for integer-s this term has no effect. The one-dimensional Heisenberg Hamiltonian is also rewritten in terms of $\vec{l}$ and $\vec{\phi}$:

$$\sum_i 2Js^2\hat{S}_i\cdot\hat{S}_j \rightarrow s^2\int dx[-1+(1/2)(d\vec{\phi}/dx)^2+2\vec{l}^2/s^2]$$
$$= v\int dx[(g/2)\vec{l}^2+(1/2g)(d\vec{\phi}/dx)^2] + constant \tag{8}$$

with $v = 4Js$ and $g = 2/s$. Including the time-derivitive term, we obtain the Lagrangian in the form:

$$L = \int dx[\vec{l} \cdot (\vec{\phi} \times \partial\vec{\phi}/\partial t) - (vg/2)\vec{l}^2 - (v/2g)(\partial\vec{\phi}/\partial x)^2] \tag{A9}$$

Note that written in this form, the Lagrangian contains only a first time-derivitive. If we replace $\vec{\phi}$ by $< \vec{\phi} >$ in the time-derivitive term then it becomes identical to the one used in Ref. (7) in the long wavelength approximation. To obtain the second-order time-derivitive term of Eq. (2.3) we simply eliminate $\vec{l}$, using the Euler-Lagrange equation:

$$vg\vec{l} = \vec{\phi} \times \partial\vec{\phi}/\partial t \tag{A10}$$

This is equivalent to integrating out $\vec{l}$ in the path-integral where it appear quadratically. This gives a new term in L_1 of the form:

$$L_{kinetic} = (1/2vg)(\vec{\phi} \times \partial\vec{\phi}/\partial t)^2 \tag{A11}$$

Finally, using the large-s result $|\vec{\phi}|^2 = 1$, we may replace

$$(\vec{\phi} \times \partial\vec{\phi}/\partial t)^2 \rightarrow (\partial\vec{\phi}/\partial t)^2 \tag{A12}$$

Thus we see that the first and second-order time-derivitive forms of the Lagrangian are actually equivalent. The difference between the results of the present approach, and those of Ref. (8) lies in the passage from hard to soft spins. The approach that we have taken consists of beginning with the Lagrangian in second-order form, Eq. (2.3) and then relaxing the constraint of the field $\vec{\phi}$ and introducing a phenomological potential energy with quadratic and quartic terms. The approach of

Ref. (8) amounts to beginning with the Lagrangian in first order form, Eq. (A9) and then following the same steps (the constraint $\vec{l} \cdot \vec{\phi} = 0$ also being relaxed). We may still eliminate $\vec{l}$ after removing the constraint. However, the kinetic term is now $(1/2vg)(\vec{\phi} \times \partial\vec{\phi}/\partial t)^2$ rather than $(1/2vg)(\partial\vec{\phi}/\partial t)^2$. These two forms are no longer equivalent with the constraint removed. If we replace $\vec{\phi}$ by $< \vec{\phi} >$ in the kinetic term then we obtain the term that is effectively used in Reference (8). This alternative form of the Lagrangian contains, to quadratic order, no time derivitives of the longitudinal component of $\vec{\phi}$. Consequently the Euler-Lagrange equation $\delta L/\delta\phi_L = 0$ becomes a constraint equation. For a standard Néel state it simply imposes the constraint $\phi_L = 0$, but in the triangular lattice case where the Lagrangian contains cross-terms between longitudinal and transverse components of $\vec{\phi}$ the constraint determines the longitudinal component of ϕ to be proportional to the transverse part. Thus the number of excitations is not increased relative to ordinary spin-wave theory; there is no extra branch. However the mixing in of the longitudinal component with the transverse ones can substantially modify the dispersion relation and intensities.

Which of these approaches is correct? We present arguments here in favour of the approach used in this paper. First of all, as discussed in Section 3, the passage from hard-spin to soft-spin models can be accomplished using the large-n limit of the $O(n)$ non-linear σ-model. Using this approach the kinetic energy has the $(\partial\vec{\phi}/\partial t)^2$ form. Indeed, a Lagrangian density of the form:

$$\mathcal{L} = (1/2v)(\vec{\phi} \times \partial\vec{\phi}/\partial t)^2 - (v/2)(\partial\vec{\phi}/\partial x)^2 + ... \tag{A13}$$

is not Lorentz invariant. The spin-wave velocity is no longer v but is rather given by $v/ < \phi >$. Thus as we decrease the interchain coupling the velocity increases

and would actually diverge at the critical point in the Néel case. The disordered phase would not contain harmonic magnon excitations. If we begin with a Lorentz-invariant hard-spin long-wavelength theory, such as the non-linear σ-model then we should expect that whatever renormalization processes produce an effective soft-spin model should preserve the Lorentz invariance, and hence not change the spin-wave velocity. Including small breaking of Lorentz-invariance some renormalization of the spin-wave velocity would occur but there is no reason to expect it to diverge at the critical point. A possible solution to this problem might be to also modify the spatial derivitive term, taking a Lagrangian density of the form:

$$\mathcal{L} = (1/2v)(\vec{\phi} \times \partial\vec{\phi}/\partial t)^2 - (v/2)(\vec{\phi} \times \partial\vec{\phi}/\partial x)^2 + ... \tag{A14}$$

This is now Lorentz-invariant and the spin-wave velocity no longer depends on $< \phi >$. However the disordered phase would again not contain harmonic magnons. Furthermore, there is no reason why the $(\partial\vec{\phi}/\partial x)^2$ term, present in the hard-spin Lagrangian, should be excluded from the soft-spin Lagrangian.

From a more general perspective, $(\partial\vec{\phi}/\partial x)^2$ and $(\partial\vec{\phi}/\partial t)^2$ are a couple of perfectly good terms which respect all the symmetries of the problem and there is no reason to exclude them from the Lagrangian. The same is true of $(\vec{\phi} \times \partial\vec{\phi}/\partial t)^2$ and $(\vec{\phi} \times \partial\vec{\phi}/\partial x)^2$. In general we should include all four terms (together with quartic interchain couplings) in the effective Lagrangian. The quartic terms were omitted in our treatment in the usual spirit of Landau-Ginsburg theory. If we are sufficiently close to the critical point so that $< \phi >$ is small then they are unimportant. Further from the critical point they could be included and would modify the spin-wave spectrum. (Indeed by including them with several additional free parameters we could presumably get a better fit to the experimental data.) However, they do not

change the qualitative picture presented here. In particular, as long as the $(\partial\vec{\phi}/\partial t)^2$ term is present in the Lagrangian the extra branch will be present.

Apart from these theoretical arguments, there is an experimental reason to prefer the Lagrangian used here. As discussed above, the main qualitative feature which distinguishes the present approach from the alternative of Ref. (8) and from conventional spin-wave theory is the presence of an additional excitation branch in the paramagnetic zone. We argued in Section 2 that the experimental evidence for this branch in $CsNiCl_3$ is very compelling. The presence of an xz-polarized mode at $(0,0,1)$ with a energy $2\frac{1}{2}$ times higher than that of the upper mode at $(1/3,1/3,1)$ implies the existence of a second xz-polarized branch in the paramagnetic zone since with a single branch these two modes would have to be degenerate. In both conventional spin-wave theory and in the model of Ref. (8) this degeneracy cannot be lifted by higher-order corrections due to the symmetry argument spelled out in Section 2. We note that in Ref. (8) the theory is compared only to unpolarized data. The agreement then looks very good since the extra xz branch is masked by the y-polarized branch near $(0,0,1)$. As the above discussion indicates, it is crucial to compare the theory with the polarized neutron-scattering experiments. The present theory gives an extra xz-polarized branch, albeit with an energy which is about 10% higher than experiment near $(0,0,1)$. The alternative of Ref. (8) does not contain this experimental feature at all.

In conclusion both theoretical and experimental arguments favor the Lagrangian used here with a $(\partial\vec{\phi}/\partial t)^2$ term, or perhaps better still, a combination of both types of terms.

---

*Present address: Physics Department, Princeton University, Princeton, NJ08544.

[1]F.D.M. Haldane, Phys. Lett. 93A, 464 (1983). For a review see I. Affleck, J. Phys.: Condensed Matter 1, 3047 (1989).

[2]W.J.L. Buyers, R.M. Morra, R.L. Armstrong, P. Gerlach and K. Hirakawa, Phys. Rev. Lett. 56, 371 (1986); R.M. Morra, W.J.L. Buyers, R.L. Armstrong and K. Hirakawa, Phys. Rev. B38, 543 (1988).

[3]I. Affleck, Phys. Rev. Lett. 62, 474, E 1927 (1989); 65, 2477, 2835 (1990).

[4]See, for example, S.-K. Ma, *Modern Theory of Critical Phenomena* (Benjamin-Cummings, London, 1976).

[5]T. Garel and P. Pfeuty, J. Phys. C9, L245 (1976); D. Bailin, A. Love and M.A. Moore, J. Phys. C10, 1159 (1977).

[6]K. Kakurai, M. Steiner and J.K. Kjems, J. Phys.: Cond. Matt. 3, 715 (1991).

[7]Z. Tun, W.J.L. Buyers, A. Harrison and J.A. Rayne, Phys. Rev. B43, 13331 (1991).

[8]M.L. Plumer and A. Caillé, Phys. Rev. Lett. 68, 1042 (1992).

[9]See, for example, C. Kittel, *Quantum Theory of Solids* (Wiley, New York, 1963).

[10]A. Harrison, M.F. Collins, J. Abu-Dayyeh and C.V. Stager, Phys. Rev. B43, 679 (1991).

[11]S. Coleman, R. Jackiw and H.D. Politzer, Phys. Rev. D10, 2491 (1974).

[12]G.F. Wellman, Undergraduate Thesis, University of British Columbia, 1991, unpublished.

[13]H.J. Schulz, Phys. Rev. B34, 6372 (1986). K. Katsumata, H. Hori, T. Takeuchi, M. Date, A. Yamagishi and J.P. Renard, Phys. Rev. Lett. 63, 86 (1989). Y. Ajiro, T. Goto, H. Kikuchi, T. Sakakibara and T. Inami, Phys. Rev. Lett. 63, 1424 (1989). I. Affleck, Phys. Rev.B41, 6697 (1990); A.M. Tsvelik, Phys. Rev. B42, 10499 (1990).

[14]Z. Tun, private communication.

[15]F.D.M. Haldane, Phys. Rev. Lett.61, 1029 (1988).

FIG. 1. Orientation of spin vectors on the six inequivalent sub-lattices (See Figure 2) for the stacked triangular lattice antiferromagnet.

FIG. 2. Labelling of sites and lattice vectors in the basal plane.

FIG. 3. The reciprocal lattice, projected onto the basal plane, showing the paramagnetic Brillouin zone, the wave-vector correponding to $(\eta, \eta, 1)$ and the reflection symmetry: $\eta \rightarrow 1 - \eta$.

FIG. 4. Unit vectors in spin-space.

FIG. 5. A longitudinal fluctuation on sub-lattice A is not orthogonal to a transverse fluctuation on neighboring sub-lattice B.

FIG. 6. Dispersion relation in $CsNiCl_3$ compared to Landau-Ginsburg model: a) y-polarization, b) xz-polarization. Thick, thin and dotted lines represent strong ($I > .64$), medium ($.13 < I < .64$) or weak ($I < .13$) relative intensity, where the intensity is normalized to one for the y-mode at $(0, 0, 1)$. (See Figure 7.)

FIG. 7. Intensites from Landau-Ginsburg model for $CsNiCl_3$. Curves 1,2,3 and 4 refer to xz-polarized modes noted in Figure 6b.

FIG. 8. Dispersion relation in $CsNiCl_3$ with xz-polarization compared to conventional spin-wave theory.

FIG. 9. Dispersion relation in $RbNiCl_3$ compared to Landau-Ginsburg model. Thick, thin and dotted lines represent strong ($I > .64$), medium ($.13 < I < .64$) or weak ($I < .13$) relative intensity, where the intensity is normalized to one for the y-mode at $(0, 0, 1)$. (See Figure 10.)

FIG. 10. Intensites in Landau-Ginsburg model. Curves 1,2,3 and 4 refer to xz-polarized modes noted in Figure 9.

FIG. 11. Renormalization group flow for $O(3) \rightarrow O(2)$ universality class in four dimensions.

FIG. 12. Renormalization group flow for triangular lattice antiferromagnets in four dimensions.

FIG. 13. Dispersion relation of y-polarized mode in a magnetic field of $h = 0$ and $h = 6T$, according to spin-wave theory and Landau-Ginsburg model.

FIG. 14. Field dependence of y-polarized spin-wave frequencies at wave-vector $(0, 0, 1)$ in $CsNiCl_3$, compared to Landau-Ginsburg model.

FIG. 15. Field dependence of y-polarized spin-wave frequencies at wave-vector $(.1, .1, 1)$ in $CsNiCl_3$, compared to Landau-Ginsburg model.

FIG. 16. Field dependence of y-polarized spin-wave frequencies at wave-vector $(.39, .39, 1)$ in $CsNiCl_3$, compared to Landau-Ginsburg model.

FIG. 17. Field dependence of xz-spin-wave frequencies at wave-vector $(0, 0, 1)$ in $CsNiCl_3$, compared to Landau-Ginsburg model.

FIG. 18. Field dependence of xz-spin-wave frequencies at wave-vector $(.1, .1, 1)$ in $CsNiCl_3$, compared to Landau-Ginsburg model.

FIG. 19. Field dependence of xz-spin-wave frequencies at wave-vector $(.39, .39, 1)$ in $CsNiCl_3$, compared to Landau-Ginsburg model.

FIG. 20. Classical path traced out on the unit sphere by time-evolution of spin variable.

FIG. 21. The change in the area resulting from an infinitesimal deformation of the path.

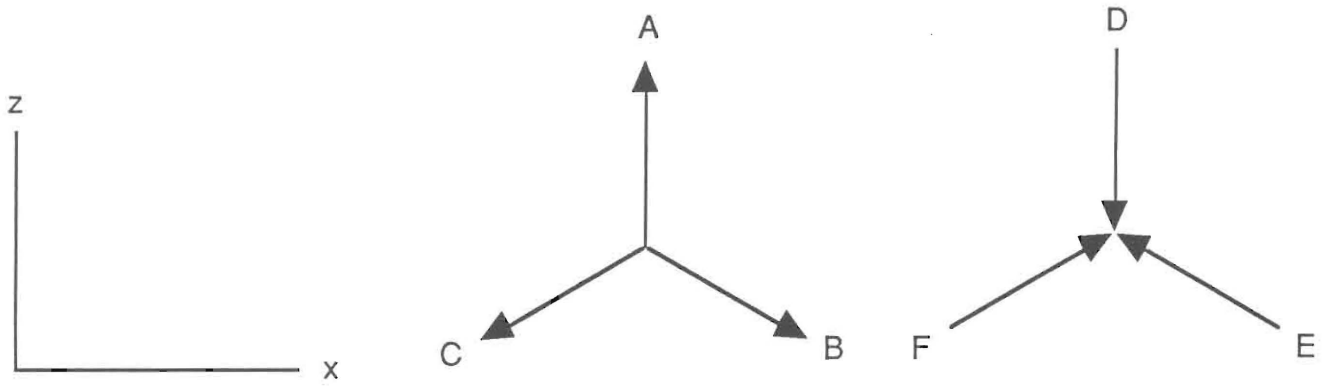

Figure 1

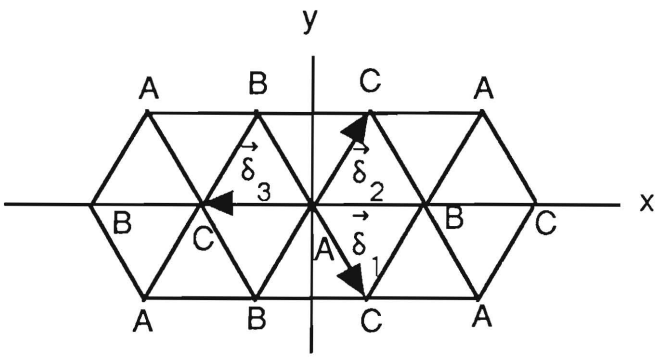

Figure 2

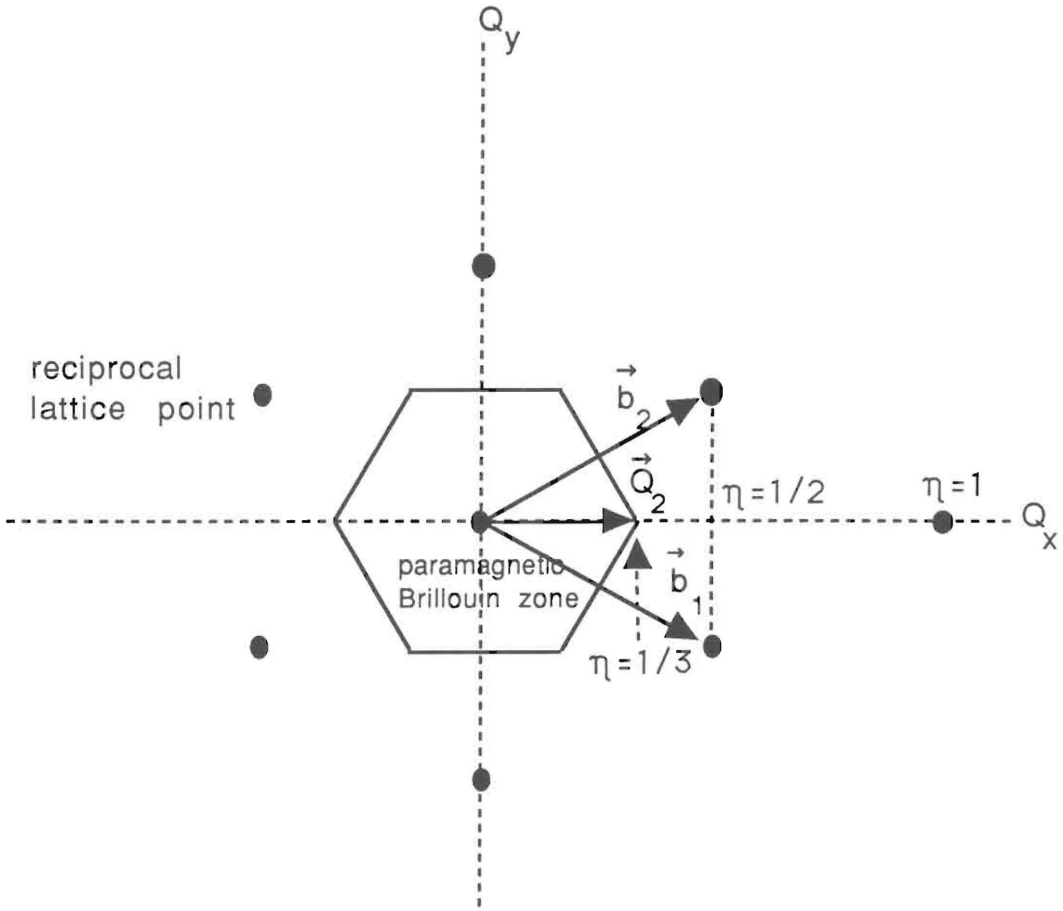
Q_y
reciprocal
lattice point
$\vec{b}_2$
$\vec{Q}_2$
$\eta = 1/2$
$\eta = 1$
Q_x
paramagnetic
Brillouin zone
$\vec{b}_1$
$\eta = 1/3$

Figure 3

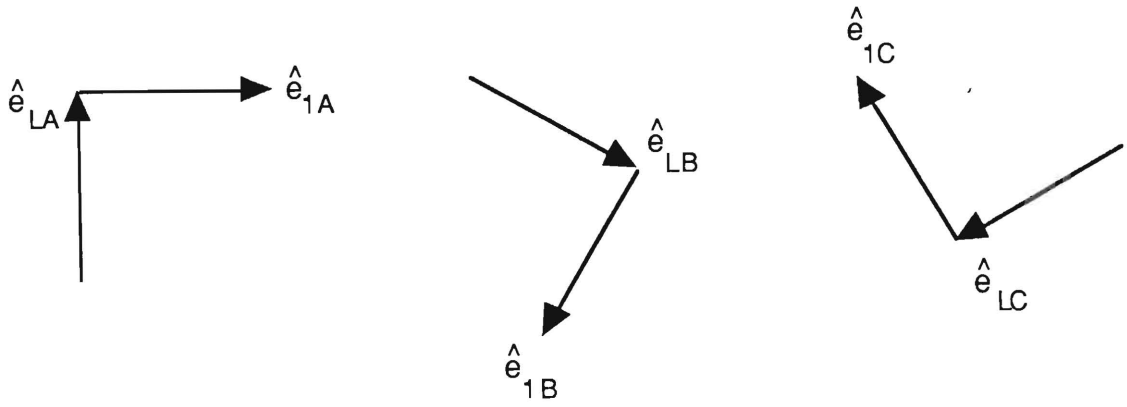

Figure 4

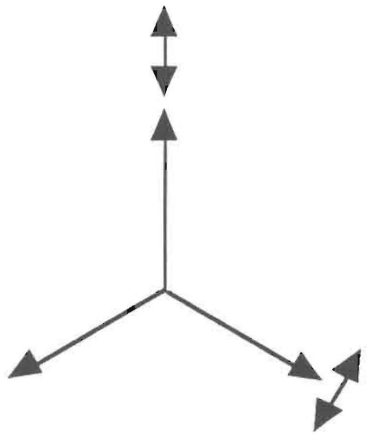

Figure 5

Spin-wave frequencies for y-polarization: $CsNiCl_3$ data vs. theory

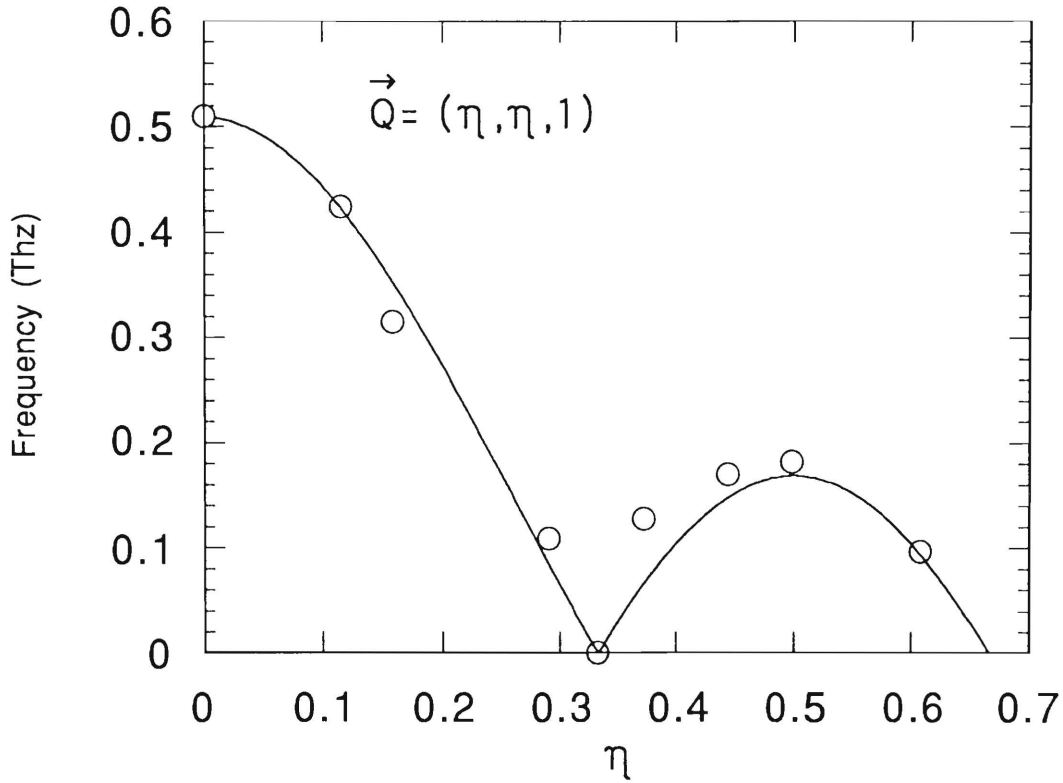

Figure (6a)

Spin-wave frequencies for xz-polarization: $CsNiCl_3$ data vs. Landau-Ginsburg Theory

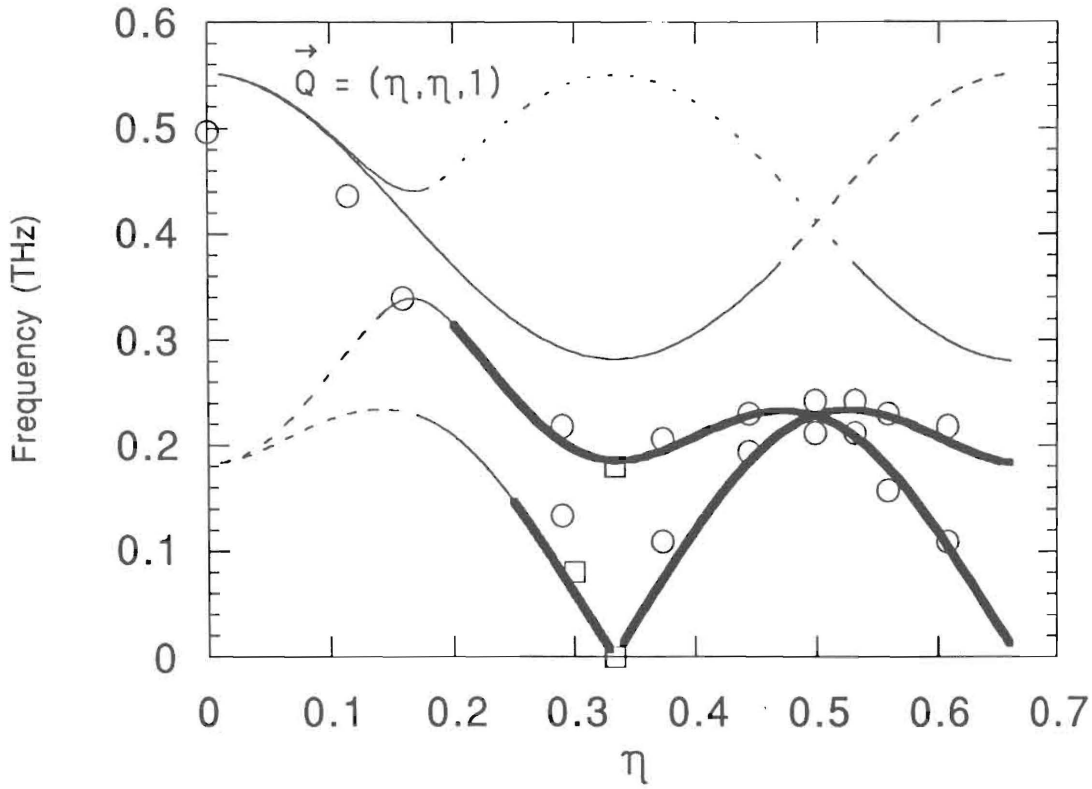

Figure (6b)

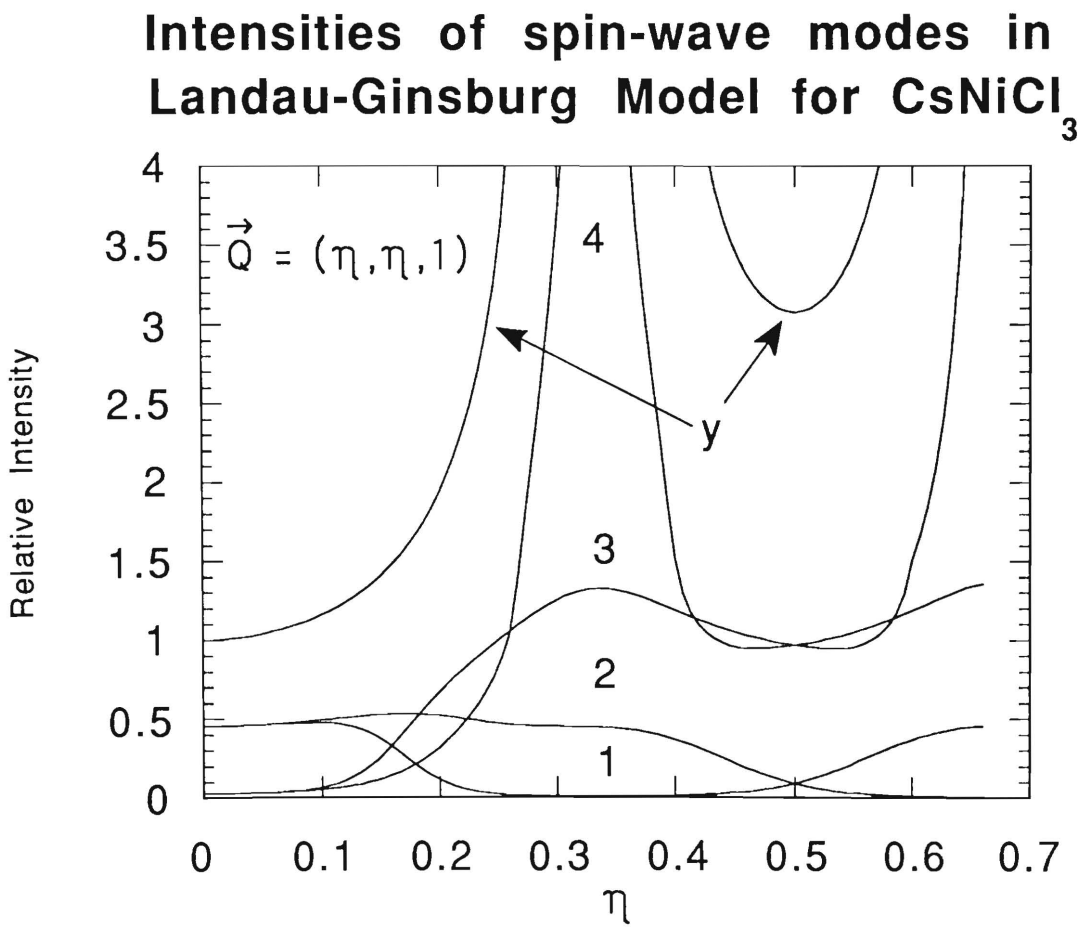
Intensities of spin-wave modes in
Landau-Ginsburg Model for CsNiCl3
Relative Intensity
η
Q = (η,η,1)
y
1
2
3
4
0
0.5
1
1.5
2
2.5
3
3.5
4
0.1
0.2
0.3
0.4
0.5
0.6
0.7

Figure (7)

Spin-wave frequencies for xz-polarization: $CsNiCl_3$ data vs. conventional spin-wave theory

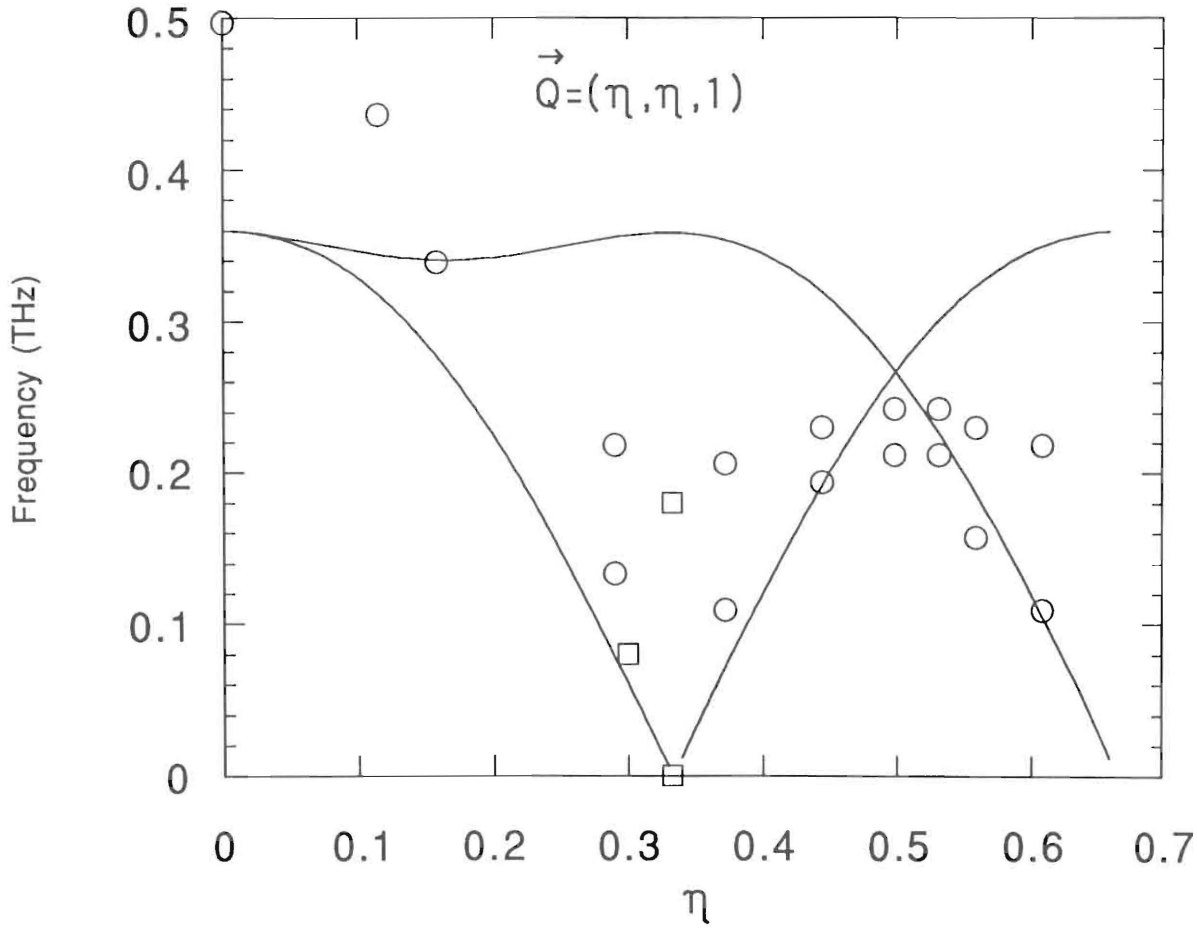

Figure (8)

Spin-wave frequencies: Landau-Ginsburg Model vs. $RbNiCl_3$ Data

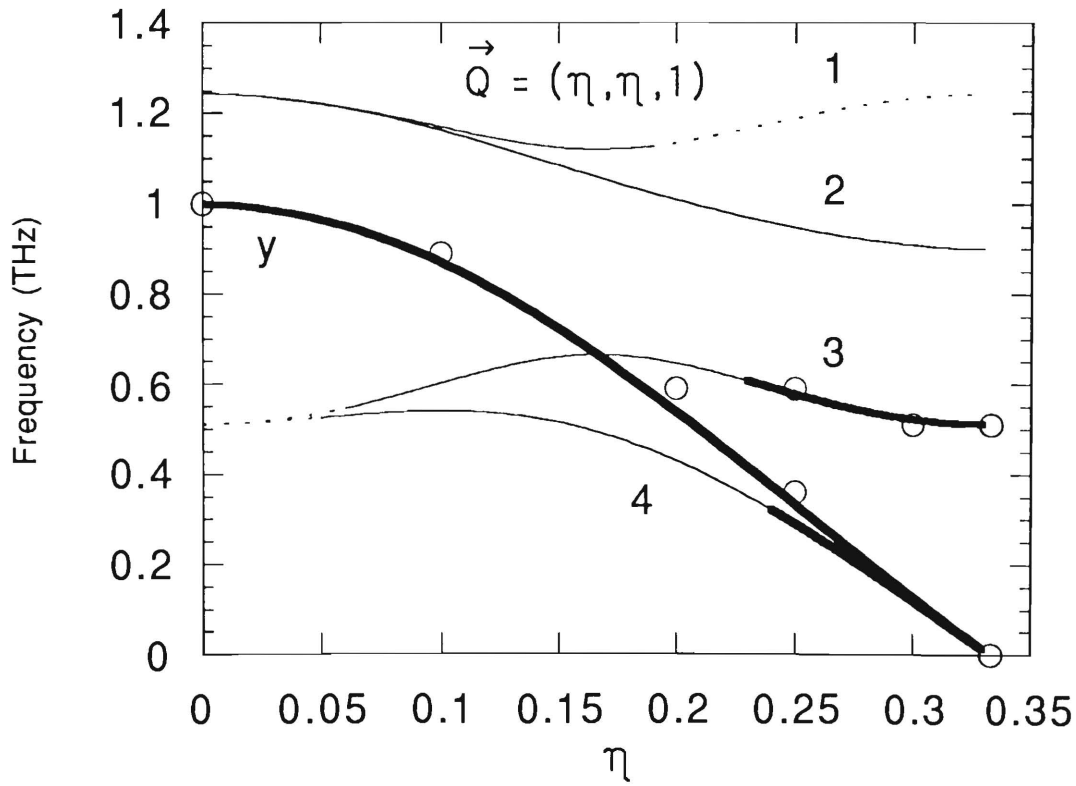

Figure (9)

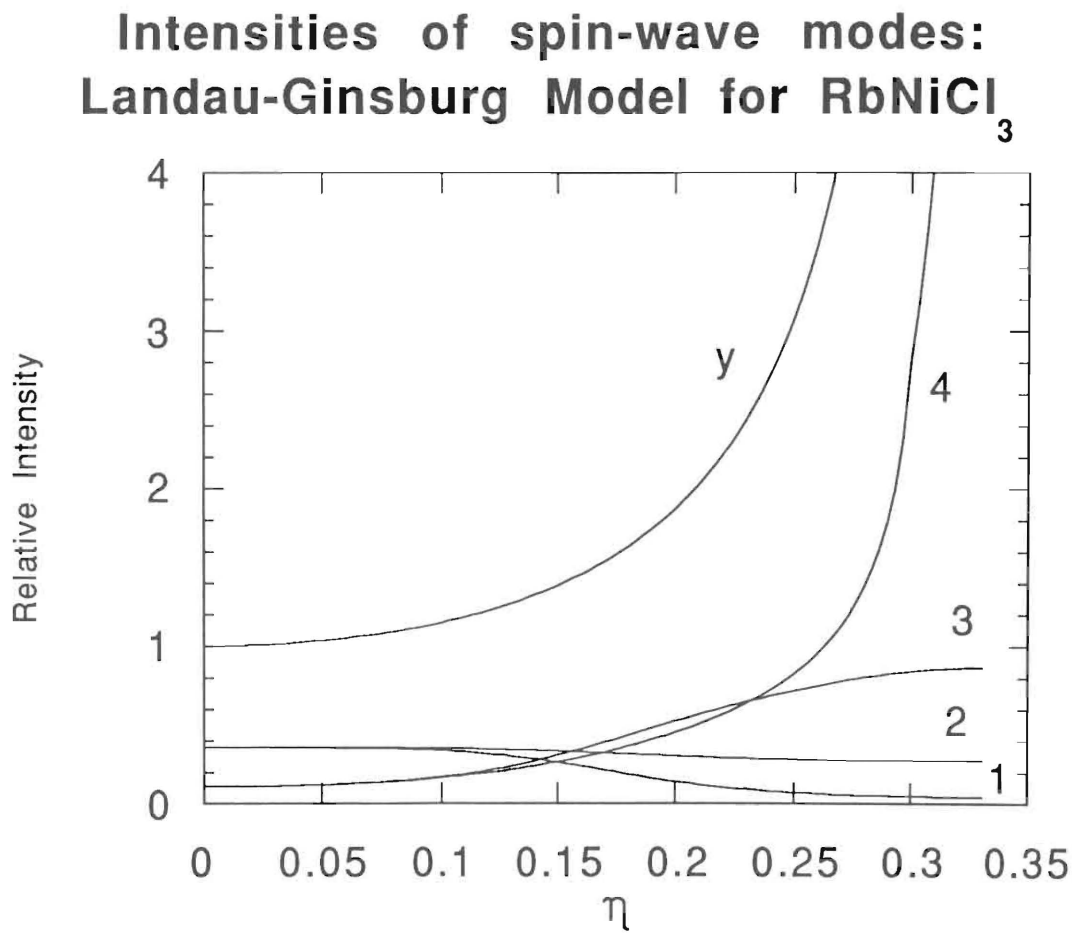
Intensities of spin-wave modes:
Landau-Ginsburg Model for RbNiCl3
Relative Intensity
η
y
1
2
3
4
0
1
2
3
4
0
0.05
0.1
0.15
0.2
0.25
0.3
0.35

Figure (10)

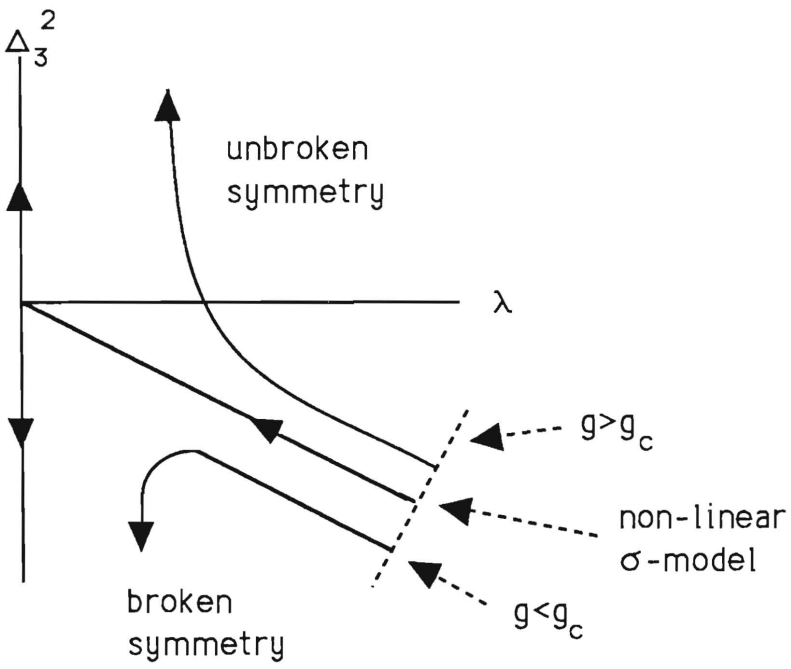
Δ_3^2
unbroken
symmetry
λ
$g>g_c$
non-linear
σ-model
broken
symmetry
$g<g_c$

Figure 11

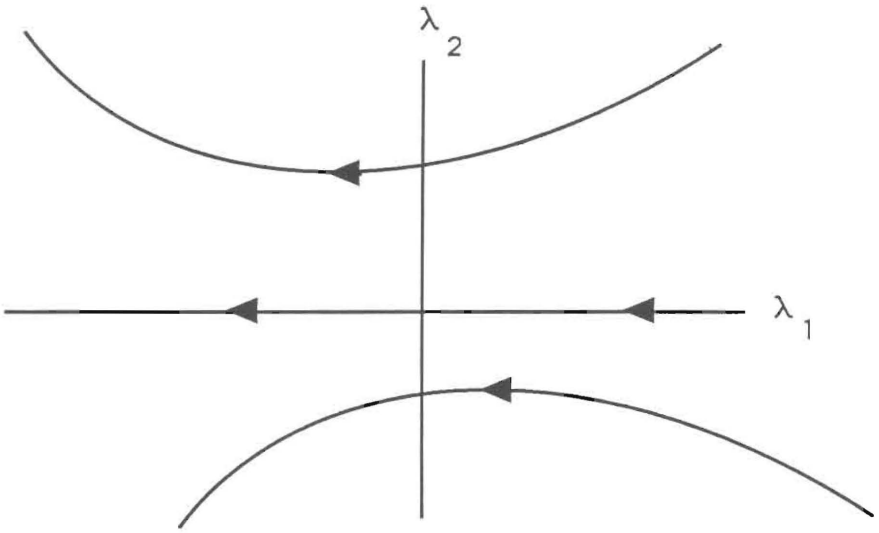

Figure 12

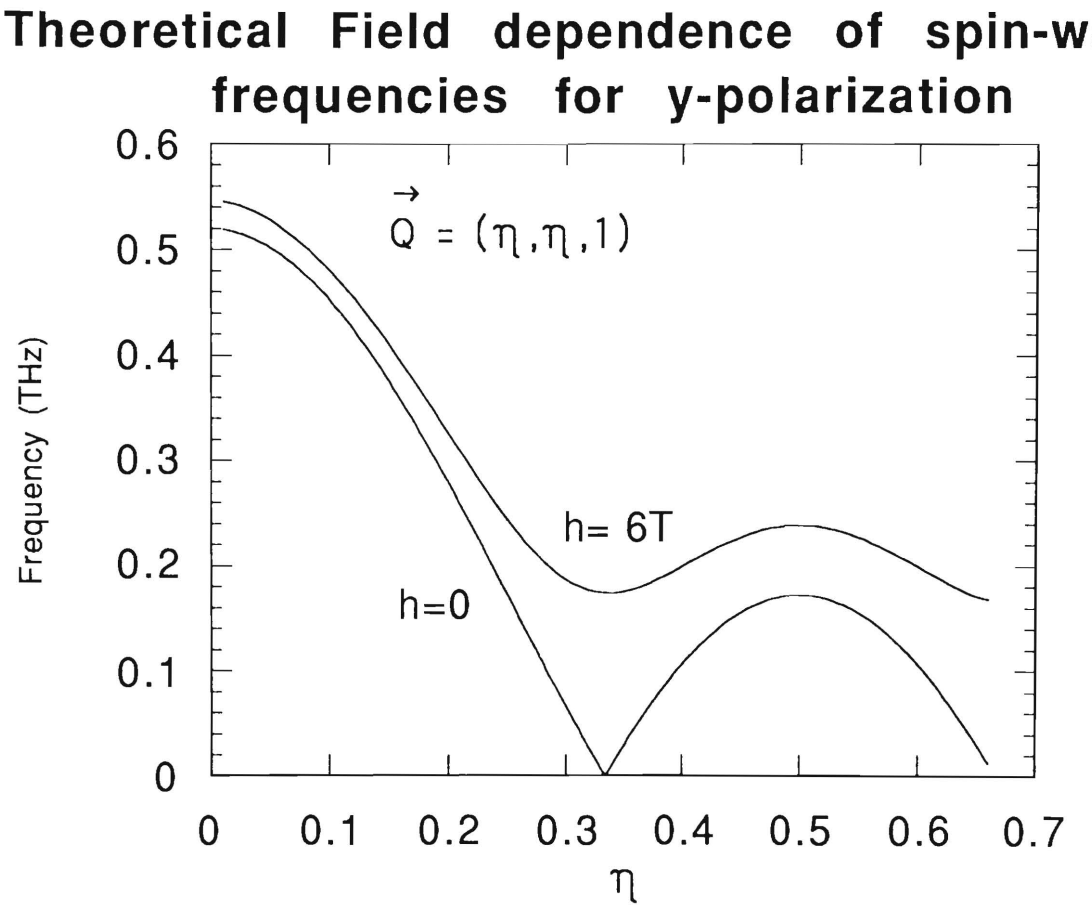
Theoretical Field dependence of spin-wave frequencies for y-polarization
Frequency (THz)
0.6
0.5
0.4
0.3
0.2
0.1
0
0
0.1
0.2
0.3
0.4
0.5
0.6
0.7
η
Q = (η,η,1)
h= 6T
h=0

Figure (13)

Field-dependence of spin-waves: $CsNiCl_3$ data vs. Landau-Ginsburg Model

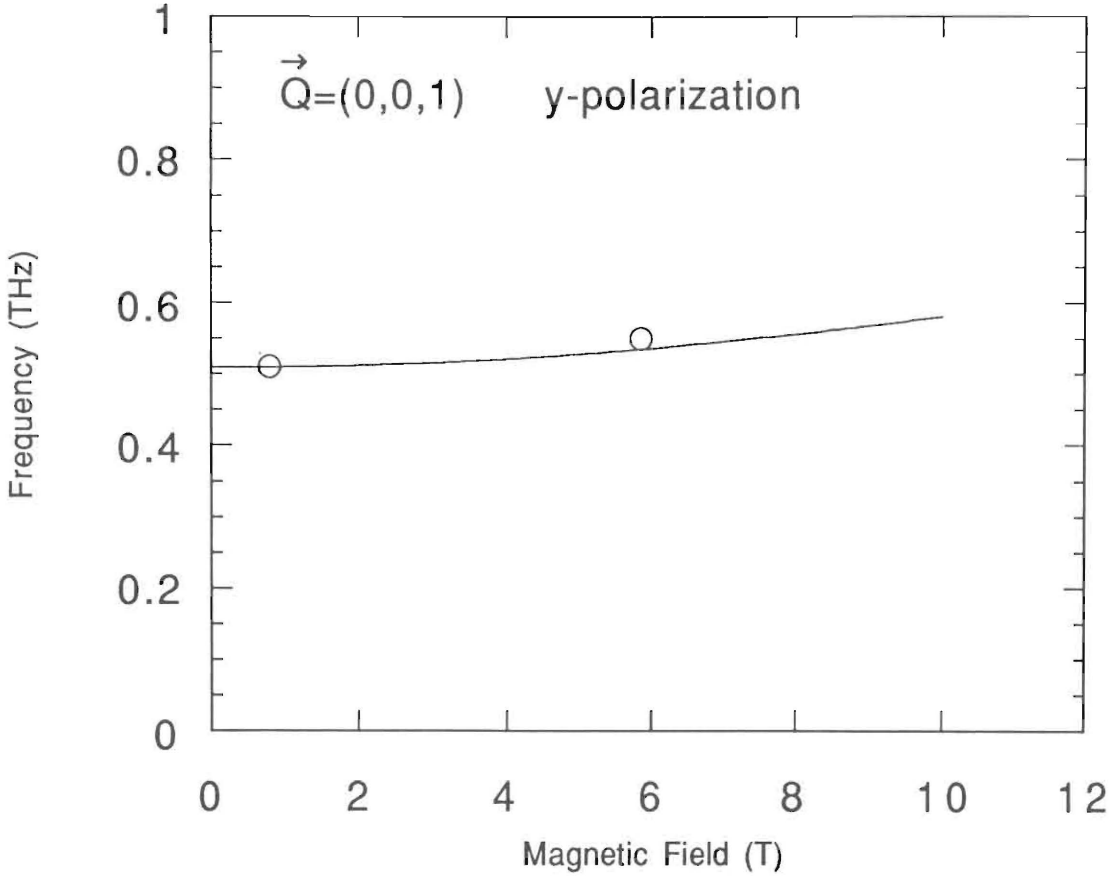

Figure (14)

Field-dependence of spin-wave frequencies: $CsNiCl_3$ data vs. Landau-Ginsburg Model

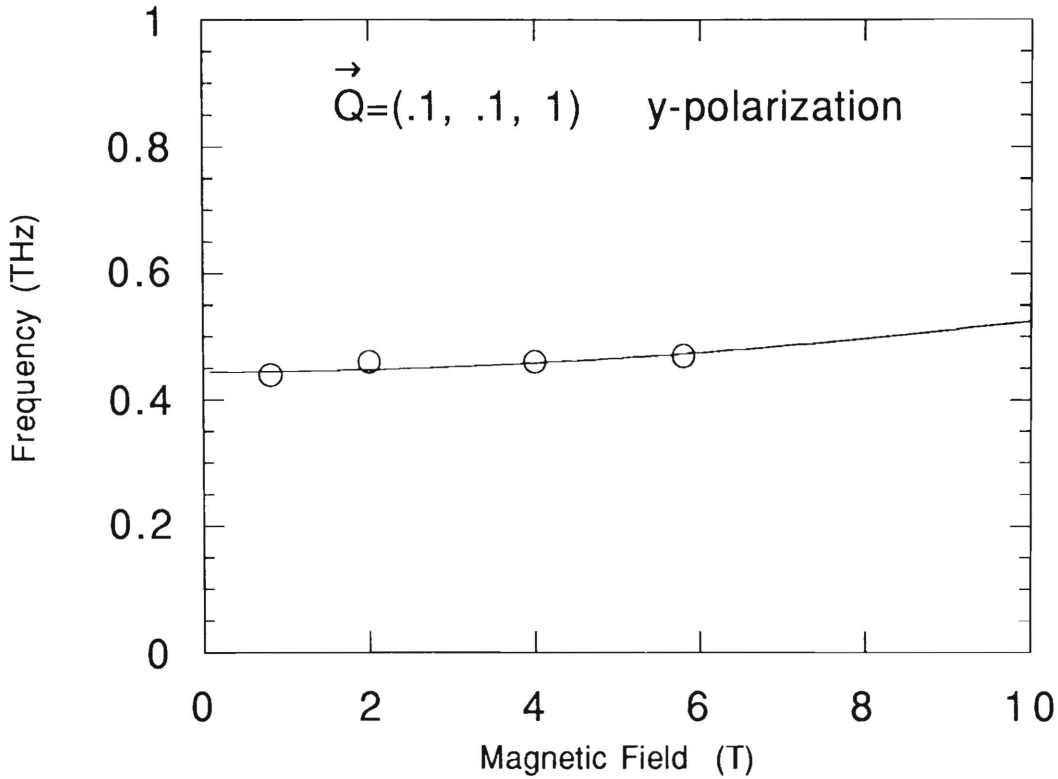

Figure (15)

Field-dependence of spin-wave frequency: $CsNiCl_3$ data vs. Landau-Ginsburg Model

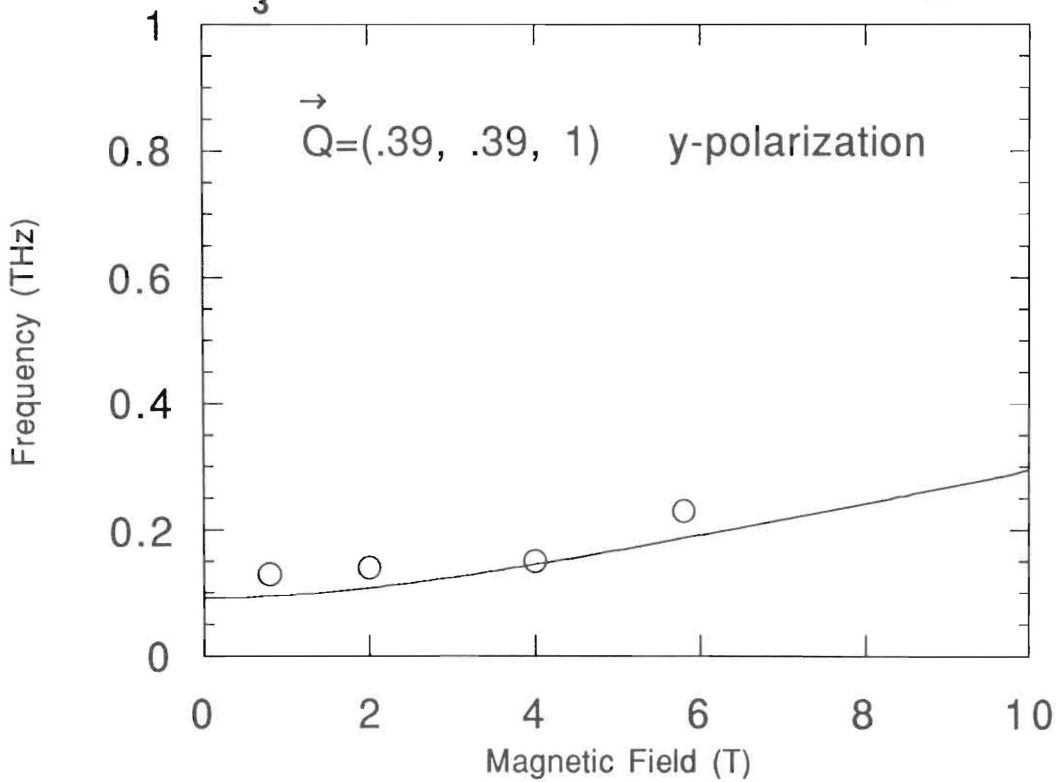

Figure (16)

Field Dependence of spin-waves: $CsNiCl_3$ data vs. Landau-Ginsburg Model

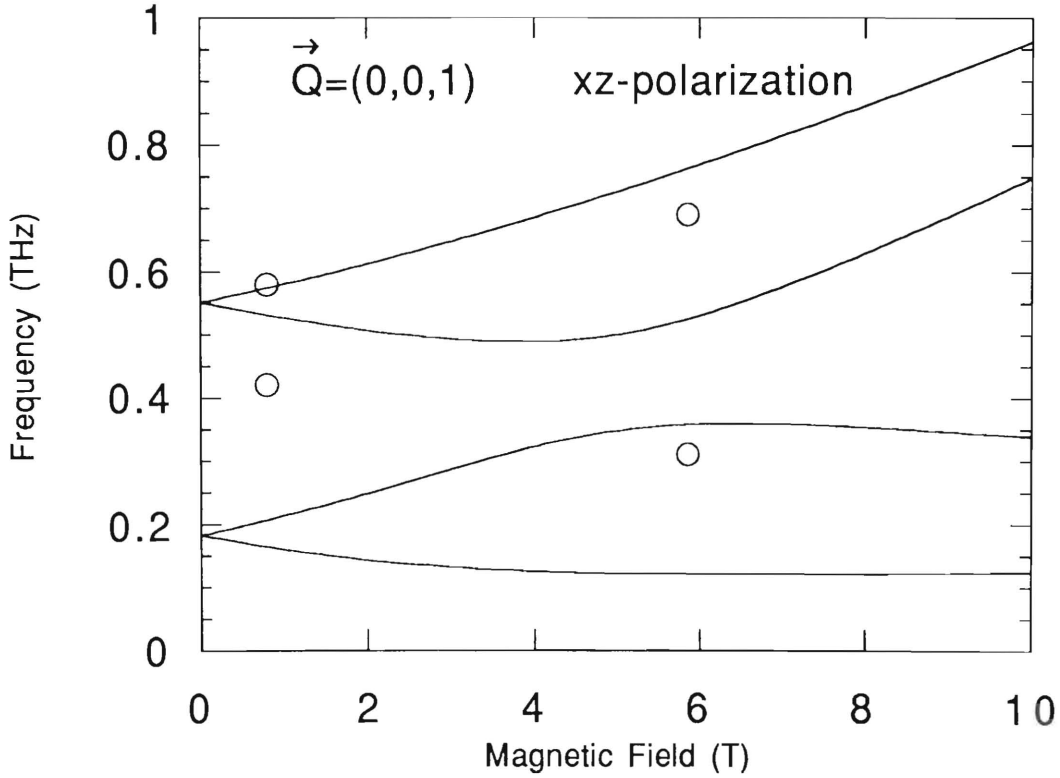

Figure 17

Field-dependence of spin-wave frequency: $CsNiCl_3$ data vs. Landau-Ginsburg Model

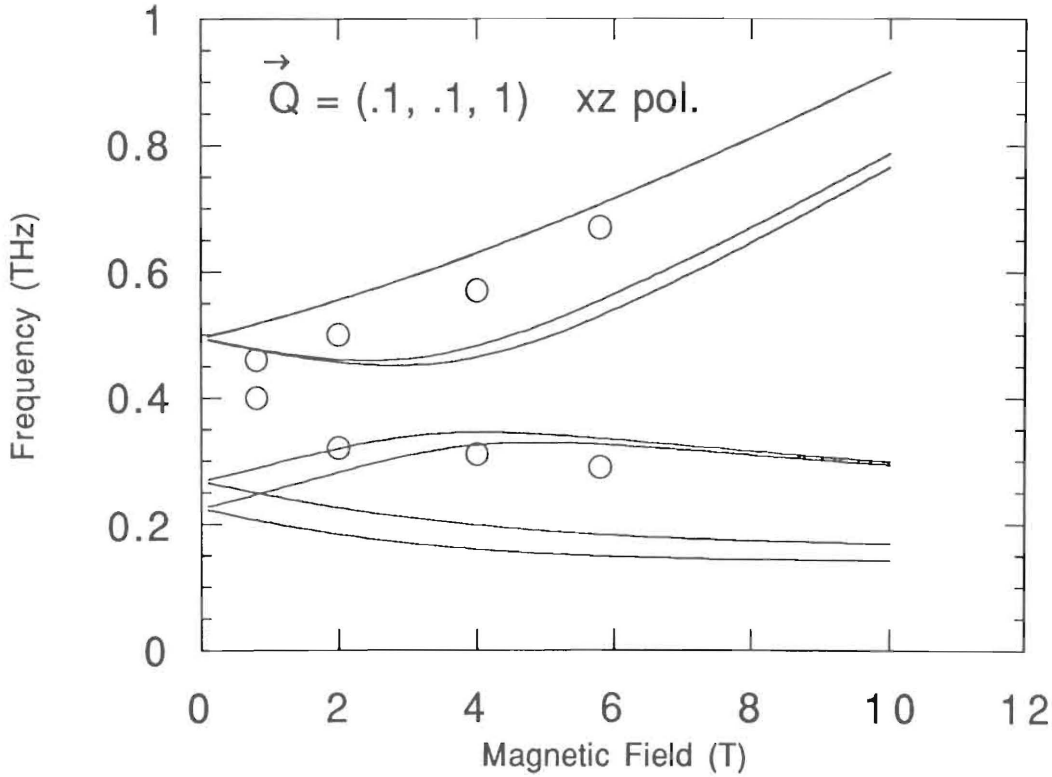

Figure (18)

Field-dependence of spin-wave frequency: $CsNiCl_3$ data vs. Landau-Ginsburg Model

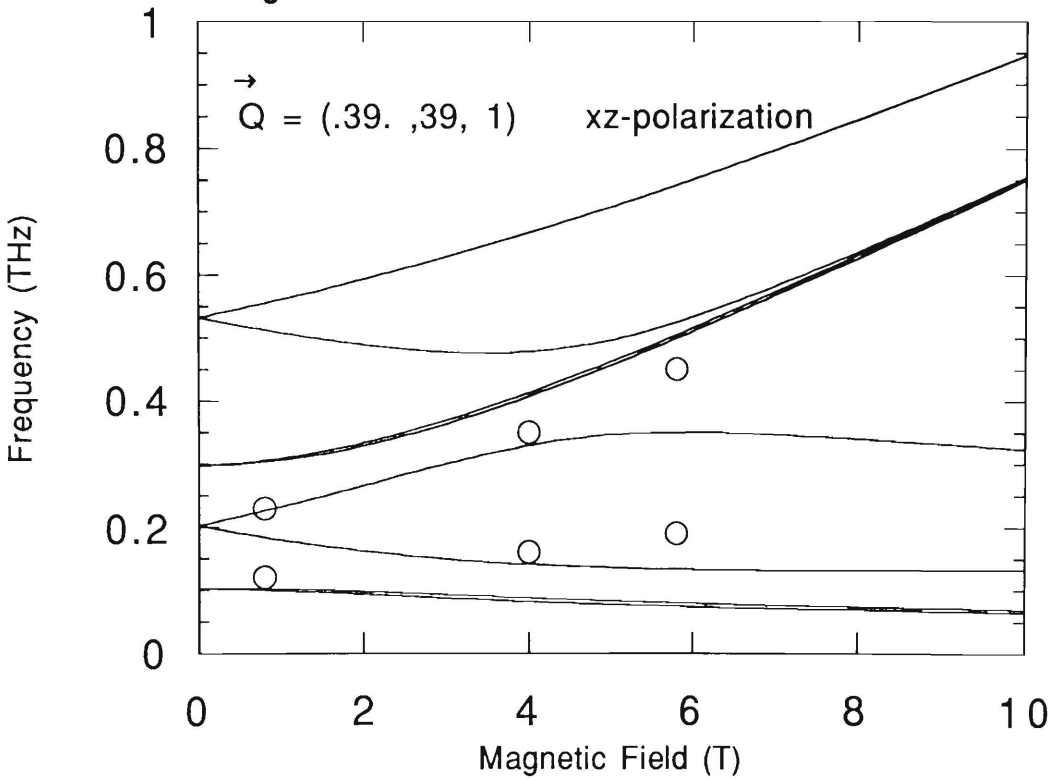

Figure 11a)

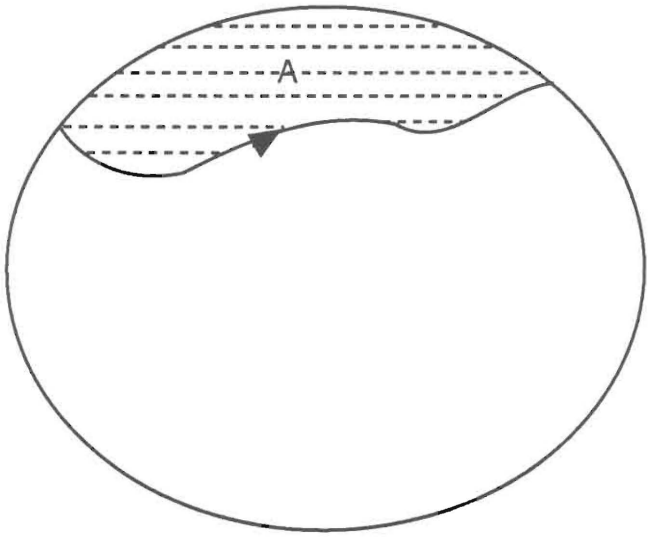

Figure 20

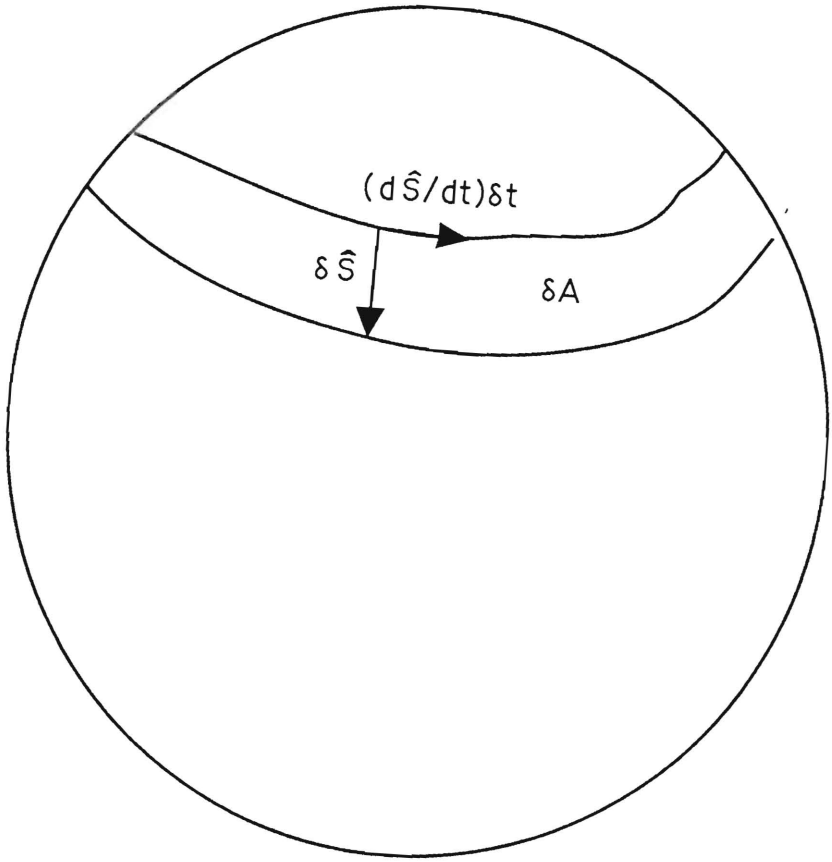

Figure 21